Spatio-Temporal Koopman Decomposition for Mechanical Vibrations and Modal Analysis

Author

Andreas Tuor[1] andre@tuor.net
Not affiliated, former position: FHNW-ISE[2]

Abstracts

In many mechanical, electrical, and general physical systems evolving over time or space, spectral analysis methods as Fast Fourier Transform (FFT), Short Term Fourier Transform (STFT), Power Spectrum Density (PSD) plays a very important role. They allow an extraction of required information content from signals in another base by decomposing it in its spectral components for further processing.
In theory this approach is very powerful, even in some 'simple' or 'not too complicated' practical cases it has proven its utility and efficiency. However, for real-world applications such as mechanical modal analysis of large dimension systems including damping, noise, and unpredictable excitation, those signals are often so complex that it can be almost impossible to obtain a high-resolution spectral decomposition with these methods due to the time-bandwidth limitation and the spectral spread/distortion introduced by discretisation and filtering (eg. the Lorenz kernel).

In a previous paper, we described how to apply High Order Dynamical Mode Decomposition (HODMD) and Kernel Density Spectrum (KDS) as alternative approach to FFT based methods to extract the different temporal vibration modes of a railway wheel axle. In this paper we will extend our analysis to spatial modes to extract the mechanical shapes of those vibrations. This is done applying a whole spatio-temporal mode decomposition (STKD) approach, the spatial decomposition part being simply the pendent of the temporal one.

Keywords: DMD, HODMD, STKD, KDS, FFT, PSD

1. Introduction

Modal vibration analysis can be performed as modal decomposition of measured displacements, velocities, or accelerations. Generally, this is done on a time dependent signal. But for mechanical systems, those vibrations are always (even if not seen), accompanied by mechanical modes distributed along the analysed structure. Simply remember the vibrating wire where you can observe traveling waves defined both in time and space.

In a first paper [1], we described how to use an approach called Higher Order Dynamic Mode Decomposition (HODMD) to extract the different temporal vibration modes, and compare it to the classical FFT based approaches. In this paper, we will use a more exhaustive approach called Spatio-Temporal Koopman Decomposition described in [2]-[8]. It can be used if we need to analyse a dataset in a multidimensional space. In this case we use it to extract both, the temporal and the spatial modes appearing on a railway wheel axel. It can be seen as a natural expansion to HODMD.

For flexibility and data availability, this analysis is done on simulation of a mechanical system. In a further paper we will transfer this approach to real measured data.

This paper is organised as follows: first we will give a rough mathematical overview of the STKD method, secondly, we will describe the mechanical system and the simulations, in a third part we will apply the STKD, and finally we will analyse the results.

2. Method (DMD-HODMD-STKD)

This section will give a brief intuitive summary of the DMD, HODMD and STKD decomposition. For more details the reader should consult the references [2] to [8].

DMD algorithm was first introduced and named by P.J. Schmid in 2008 to identify high-dimensional spatio-temporal coherent structures in (non-linear) fluid flow dynamics. It is a purely data-driven approach, no knowledge of the dynamic of the system or its governing differential equations is required.

To quote [1]:
p. 2: "The method (DMD) can be thought of as an ideal combination of spatial dimensionality-reduction techniques, such as the proper orthogonal decomposition (POD), with Fourier transform in time" and
p. 236: "DMD may be formulated as an algorithm to identify the best-fit linear dynamical system that advances high-dimensional measurements forward in time. In this way, DMD approximates the Koopman operator restricted to the set of direct measurements of the state of a high-dimensional system".

Using an approach developed for non-linear system for "simple" vibration analysis (approximated as linear problem) may sound over tuned. But we must bear in mind that we are dealing with complex high-dimensional systems where linearity can be hidden in this complexity or may even not being guaranteed anymore for large displacements.

As pointed out in [3], classical DMD suffers from a very restricting practical aspect: it fails if temporal complexity (N) is larger than spatial complexity (M). Under complexity we understand the number of frequencies, waves, or modes. In other words, it is necessary to use HODMD when the number of time-frequencies modes N is large compared to the number of spatial-frequencies modes M. This failing condition rapidly appears if a small number of sensors is used.

To overcome this restriction, references [2]-[4] introduces HODMD as an extension of DMD [5]-[7]. It can be understood as a tool to analyse high-dimensional non-linear dynamic systems in their phase-state (or state-space).

In this paper we focus on STKD algorithms described in [2], [7] and the related scripts (Octave/Matlab).

2.1 The classical Dynamic Mode Decomposition (DMD)

DMD is a purely data-driven algorithm, consisting in a regression of a dataset representing the dynamic of a system which is considered as locally (timely and spatially) linear [2].

The easiest way to describe this approach it is by a simple mathematical description. Let us consider a 1-dimensional dynamical system, $\vec{y}$ representing its states (in some cases directly the signals as positions, velocities, or measured accelerations in the case of a mechanical system), $\vec{x}$ is a spatial coordinate (can be omitted for a non-spatial depending system), t the time, f the system itself and μ the parameter(s). Its dynamics is given by a set of continuous or discrete formulated linear or non-linear first-order coupled ordinary differential equations (remark: derivatives in this document will systematically be denoted ∂, not to confound with partial):

$$\frac{\partial \vec{y}}{\partial t} = \vec{f}(\vec{y}, \vec{x}, t, \mu) \quad or \quad \overrightarrow{y_{k+1}} = \vec{F}(\overrightarrow{y_k}, \vec{x}, \mu) \qquad (1)$$

The DMD approach takes an equation-free perspective where the dynamic is unknown, and constructs a locally linear dynamic system formulated by:

$$\frac{\partial \vec{y}}{\partial t} = \boldsymbol{\mathcal{A}}\vec{y} \quad or \quad \overrightarrow{y_{k+1}} = \boldsymbol{A}\overrightarrow{y_k} \qquad (2)$$

where $\boldsymbol{\mathcal{A}}, \boldsymbol{A}$ are respectively the matrix of the continuous- and discrete-time dynamics, also called the Koopman operator. This formulation relies on the assumption that the system time snapshots lie in the invariant subspace under the action of the Koopman group [8], [9], and therefore all linear operation (especially the time-shift, readers familiar with quantum mechanics will appreciate this fact and should think about the time-shift operator…) applies to it.

The general solution for those systems corresponds to a sum of oscillations (as expected in the vibration analysis we want to perform) multiplied by some components containing the exponential decay. This solution is given by its initial condition $\overrightarrow{y_0}$ and:

$$\vec{y}(t) = \sum_{m=1}^{M} \overrightarrow{\emptyset_m}\, e^{(\delta_m + j\omega_m)t} b_m = \boldsymbol{\Phi} e^{(\Delta + \mathrm{j}\boldsymbol{\Omega})t}\boldsymbol{b} \quad or \quad \overrightarrow{y_k} = \sum_{m=1}^{m} \overrightarrow{\emptyset_{km}}\, \lambda_m^k b_m = \boldsymbol{\Phi}\boldsymbol{\Lambda}^k\boldsymbol{b} \qquad (3)$$

$\overrightarrow{\emptyset_m}$, $\boldsymbol{\Phi}$ and $(\delta_m + j\omega_m)$, $(\Delta + \mathrm{j}\boldsymbol{\Omega}), \lambda_m, \boldsymbol{\Lambda}$ are respectively the eigenvectors and (complex) eigenvalues of the matrix $\boldsymbol{\mathcal{A}}, \boldsymbol{A}$ coefficients, b_k and $\boldsymbol{b}$ are the coordinates of the initial conditions $\overrightarrow{y_0}$ in the eigenvector basis and $\boldsymbol{A} = exp(\boldsymbol{\mathcal{A}}\Delta t)$ the time operator. The terms δ, Δ represents the damping and ω, $\boldsymbol{\Omega}$ the frequency components in linear or matrixial form respectively. To find the linear approximation of Matrix $\boldsymbol{A}$, m measurement snapshots $\boldsymbol{Y}_k$, equispaced in time, are taken. Even if, theoretically, two snapshots $[\overrightarrow{y_k}\ \overrightarrow{y_{k+1}}]$ are enough, the input is overdetermined to obtain a better "fit" of the dynamic of the system. The $\boldsymbol{Y_k}$ measurements and its time shifted version $\boldsymbol{Y_{k+1}}$ are given by:

$$\boldsymbol{Y_k} = \begin{bmatrix} | & | & & | \\ \overrightarrow{y_{t_1}} & \overrightarrow{y_{t_2}} & \cdots & \overrightarrow{y_{t_m}} \\ | & | & & | \end{bmatrix} \qquad \boldsymbol{Y_{k+1}} = \begin{bmatrix} | & | & & | \\ \overrightarrow{y_{t_2}} & \overrightarrow{y_{t_3}} & \cdots & \overrightarrow{y_{t_{m+1}}} \\ | & | & & | \end{bmatrix} \qquad (4)$$

The dynamical system and the best-fit $\widetilde{\boldsymbol{A}}$ matrix are finally given by († representing the pseudo-inverse):

$$\boldsymbol{Y_{k+1}} \approx \boldsymbol{A}\boldsymbol{Y_k} \quad \Rightarrow \quad \widetilde{\boldsymbol{A}} = \boldsymbol{Y_{k+1}}\boldsymbol{Y_k^\dagger} \qquad (5)$$

The DMD algorithm produces a low-rank eigendecomposition of the system described by the matrix $\boldsymbol{A}$. It is obtained by Proper Orthogonal Decomposition (POD) rank-reduction for a reduced order model, and optimally fits the measured signal $\overrightarrow{y_k}$ in a least-square sense so that L_2 norm $\|\overrightarrow{y_{k+1}} - \boldsymbol{A}\overrightarrow{y_k}\|_2$ is minimised across all values of k.

2.2 The Higher Order Dynamic Mode Decomposition (HODMD)

As stated previously and shown in [4], DMD fails if the temporal complexity N is larger than spatial complexity M. The authors of [3] showed that if Eq. (2) leads to Eq. (3) the converse is not true; meaning that a simple linearisation is not enough to represent the whole temporal complexity.

To overcome this limitation, they proved that a more general linear decomposition than (2) that can catch the whole temporal complexity of the system given by:

$$\frac{\partial^d \vec{y}}{\partial t^d} = \boldsymbol{\mathcal{A}_{d-1}}\frac{\partial^{d-1}\vec{y}}{\partial t^{d-1}} + \boldsymbol{\mathcal{A}_{d-2}}\frac{\partial^{d-2}\vec{y}}{\partial t^{d-2}} + \cdots + \boldsymbol{\mathcal{A}_2}\frac{\partial^2 \vec{y}}{\partial t^2} + \boldsymbol{\mathcal{A}_1}\frac{\partial \vec{y}}{\partial t} + \boldsymbol{\mathcal{A}_0}\vec{y}$$

$$\overrightarrow{y_{k+d}} = \boldsymbol{A_{d-1}}\overrightarrow{y_{k+d-1}} + \boldsymbol{A_{d-2}}\overrightarrow{y_{k+d-2}} + \cdots + \boldsymbol{A_2}\overrightarrow{y_{k+2}} + \boldsymbol{A_1}\overrightarrow{y_{k+1}} + \boldsymbol{A_0}\overrightarrow{y_k} \qquad k = 1,2,\ldots,K-d \qquad (6)$$

This formulation represents the complexity of the system to a given dimension (in this case the time t). It is also verry intuitive to understand. Under the right conditions, the differential equation can be decomposed in decoupled damped linear systems [11], representing at maximum d/2 oscillators per state y. Finally, the solutions of Eq. (6) are all in the form of Eq. (3) and all expansions of Eq. (3) satisfy Eq. (6) for appropriate d and $\boldsymbol{A_i}$. Note that latest condition is assumed "easily" achievable considering that mechanical systems have a limited number of degrees of freedom, dominant modes, and must be L_2 (energy) bounded. The main requirement to apply this algorithm is to correctly define the dimension d needed to analyse the system (not too small to catch the whole complexity, neither too large to

not overfit the system) and, probably one the trickiest part, the adequate truncation (of SVD/POD) to adequately catch only the relevant information ([7], [10]).

Finally, Eq. (6) can be reformulated through an enlarged-reduced Koopman matrix $\boldsymbol{A}^*$ to bring it back to a similar and simple linear formulation as Eq. (2) but in higher dimension:

$$\overrightarrow{y_{k+1}}^* = \boldsymbol{A}^* \overrightarrow{y_k}^* \qquad \overrightarrow{y_k}^* = \begin{bmatrix} \overrightarrow{y_k}^* \\ \overrightarrow{y_{k+1}}^* \\ \cdots \\ \overrightarrow{y_{k+d-2}}^* \\ \overrightarrow{y_{k+d-1}}^* \end{bmatrix} \qquad \boldsymbol{A}^* = \begin{bmatrix} \boldsymbol{0} & \boldsymbol{I} & \boldsymbol{0} & \cdots & \boldsymbol{0} & \boldsymbol{0} \\ \boldsymbol{0} & \boldsymbol{0} & \boldsymbol{I} & \cdots & \boldsymbol{0} & \boldsymbol{0} \\ \cdots & \cdots & \cdots & \cdots & \cdots & \cdots \\ \boldsymbol{0} & \boldsymbol{0} & \boldsymbol{0} & \cdots & \boldsymbol{I} & \boldsymbol{0} \\ \boldsymbol{A^*_0} & \boldsymbol{A^*_1} & \boldsymbol{A^*_2} & \cdots & \boldsymbol{A^*_{d-2}} & \boldsymbol{A^*_{d-1}} \end{bmatrix} \quad (7)$$

2.3 The Spatio-Temporal Koopman Decomposition (STKD)

What is called the Spatio-Temporal Koopman Decomposition is "not more" than applying the HODMD to higher dimension (>1) systems to studies multidimensional traveling waves. For dimensions higher than two, it becomes much more complex due to the needed use of tensors, but hereafter we will focus on our application which is a 2-dimensional problem (a traveling wave along a wheel axle). The mathematical foundations are well described in [3] and [4], but to resume it simply, the goal is to decompose those wheel-axle traveling waves into their temporal and spatial spectral components and amplitudes $\nu, \kappa, \delta, \omega, b, \emptyset$ used in Eq. (8):

$$\vec{y}(t,x) = \sum_{n=1}^{N} \sum_{m=1}^{M} \overrightarrow{\emptyset_{mn}}\, e^{(\nu_n + j\kappa_n)x} e^{(\delta_m + j\omega_m)t} b_{mn} \quad (8)$$

To do so, we apply the same HODMD algorithm in space and in time on an SVD reduced input dataset. This is best represented by [3], from this single decomposition of space and time dataset, the Koopman decomposition for both, spatial and temporal spectral decomposition is extracted.

$$\mathbf{Y}(t,x) = \mathbf{Y}_k^{SVD} = \sum_{r=1}^{R} \boldsymbol{X}_{nr} \boldsymbol{\sigma}_r \boldsymbol{T}_{rk} \qquad k = 1,2,\dots,K-d$$

$$\text{HODMD decomposition for space on } \widehat{\boldsymbol{X}_{nr}} = \boldsymbol{\sigma}_r \boldsymbol{X}'_{nr} \qquad \text{HODMD decomposition for time on } \widehat{\boldsymbol{T}_{rk}} = \boldsymbol{\sigma}_r \boldsymbol{T}_{rk} \quad (9)$$

$$\overrightarrow{x_{ds}^k} = \boldsymbol{A_{ds-1}} \overrightarrow{x_{ds-1}^{k-1}} + \cdots + \boldsymbol{A_1} \overrightarrow{x_1^{k-d-2}} + \boldsymbol{A_0} \overrightarrow{x_0^{k-d-1}} \qquad \overrightarrow{t_{dt}^k} = \boldsymbol{A_{dt-1}} \overrightarrow{t_{dt-1}^{k-1}} + \cdots + \boldsymbol{A_1} \overrightarrow{t_1^{k-d-2}} + \boldsymbol{A_0} \overrightarrow{t_0^{k-d-1}}$$

In the continuous domain this corresponds to the following classical differential equation system (please note that each dimension has is one related $\boldsymbol{\mathcal{A}, A}$, the same notation is used only for convenience):

$$\frac{\partial^{ds}\vec{y}}{\partial x^{ds}} = \boldsymbol{\mathcal{A}_{ds-1}} \frac{\partial^{ds-1}\vec{y}}{\partial x^{ds-1}} + \cdots + \boldsymbol{\mathcal{A}_1} \frac{\partial \vec{y}}{\partial x} + \boldsymbol{\mathcal{A}_0} \vec{y} \qquad \frac{\partial^{dt}\vec{y}}{\partial t^{dt}} = \boldsymbol{\mathcal{A}_{dt-1}} \frac{\partial^{dt-1}\vec{y}}{\partial t^{dt-1}} + \cdots + \boldsymbol{\mathcal{A}_1} \frac{\partial \vec{y}}{\partial t} + \boldsymbol{\mathcal{A}_0} \vec{y} \quad (10)$$

Once this decomposition is done, the classical HODMD analysis formulated under 2.2. is performed on both dimensions. The order of those ODEs is given by ds and dt, defining the dimension to look in. The HODMD procedure by its several SVD-truncation procedures will "search" the best "ODE dimension to fit for". It must be noted that HODMD is not an automatic "sparcifier", some manual corrections can/must be done to limit the "fit" range.

2.4 Procedure overview

Finally, the STKD algorithm can be resumed as following (see STKD code in [2]):

1. Space-time datasets reduction
   Reduce the high dimension spatio-temporal input snapshot matrix by SVD and truncation.
   From this decomposition, two reduced time and space snapshot matrices are extracted ($\widehat{\boldsymbol{X}_{nr}}$ *and* $\widehat{\boldsymbol{T}_{rk}}$ of Eq.9).
2. For each time & space dataset perform a HODMD decomposition
   Start with the dimension having the lowest number of samples and optimise the parameters for it first
   - 2.1. Create the modified snapshot matrices ($\overrightarrow{y_k}^*$ of Eq.7) by shifting the input dataset by the number of "ODE dimension d we want to observe for fit" (ODE orders of Eq.10).
   - 2.2. SVD with truncation (find the order of the ODE fitting at best the dataset) of the modified snapshot matrices.
   - 2.3. Create and SVD reduced/truncate the reduced modified snapshot matrix to create the reduced modified Koopman matrix (for Eg.7 right).
   - 2.4. Compute eigenvalues, frequencies, and growth rates of relevant dimension of formula (8).
   - 2.5. Compute the amplitudes of the relevant dimension of formula (8) (uses SVD).
   - 2.6. Optional dimension truncation on amplitude (should be analysed in detail or avoided)
   - 2.7. Compute the approximation errors on $\widehat{\boldsymbol{X}_{nr}}$ *and* $\widehat{\boldsymbol{T}_{rk}}$ (very helpful to locate the dominant error component).
3. Compute the complex exponentials of Eq. (8).
4. Optional truncation of the modes on decreasing amplitude.
5. Reconstruct the original signal and calculate the error.

The truncation limit for SVD reduction is very tricky and can be obtained by several approaches:

1. Use a standard SVD error estimation defined by a tolerance, removing all $\sigma_i < \varepsilon\sigma_1,\ 0 < \varepsilon < 1$.
2. Define the number of dominant modes N $(\sigma_1 \cdots \sigma_N)$.
3. Calculate an optimal hard threshold using the approach described in [8].

Generally, we use the third approach for real application noisy measurements, for simulations it depends on the shape of the SVD extracted sigmas. A deeper analysis concerning this truncation is required.

In this paper we use and adapt the scripts provided by [2] and [8] and use OCTAVE for the signal processing.

As mentioned, this subject is far too complex to be described in more details here. This section is intended as an overview to roughly explain “what is going one”. We strongly suggest reading [2] to [8] and apply the procedures.

3. System (mechanical structure) and simulations

The STKD procedure is applied to a railway wheel axle to extract the spatial and temporal vibration modes of the structure. To be able to gather enough data and remain flexible for adjustments, we tested this procedure on FEM simulations.

3.1 Mechanical system and simulation model

The mechanical system to analyse is a railway wheel axle encountered in bogies (Fig. 3.1.).

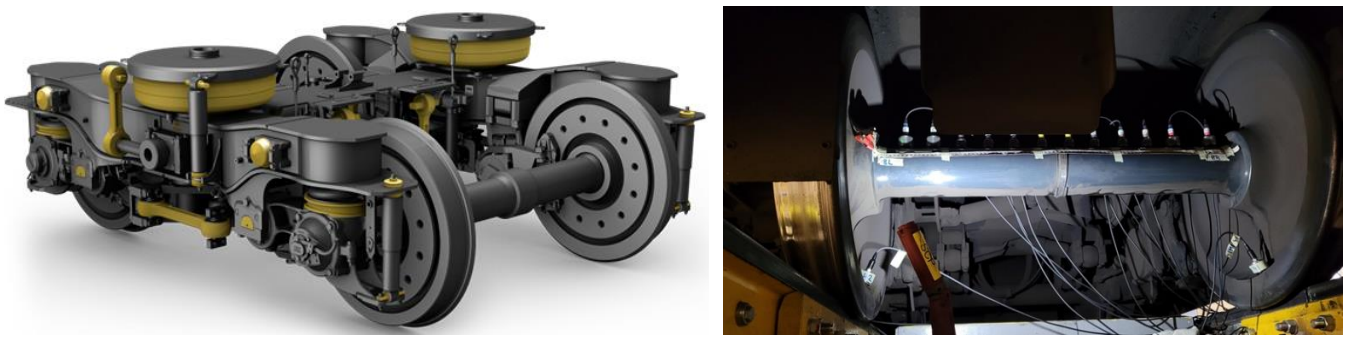

Figure 3.1: Example of a railway bogie (https://www.trelleborg.com/en/anti-vibration-solutions/your-industry/rail-and-mass-transit/bogie) and a photo showing the mounted accelerometers (vibration sensors).

On figure 3.2, we represented a schematic drawing of such an axel, and a drawing of the used FEM model. On latest, we showed the position of the virtual sensors (Sxx) where the different accelerations are extracted, as well as the location of the different applied excitations.

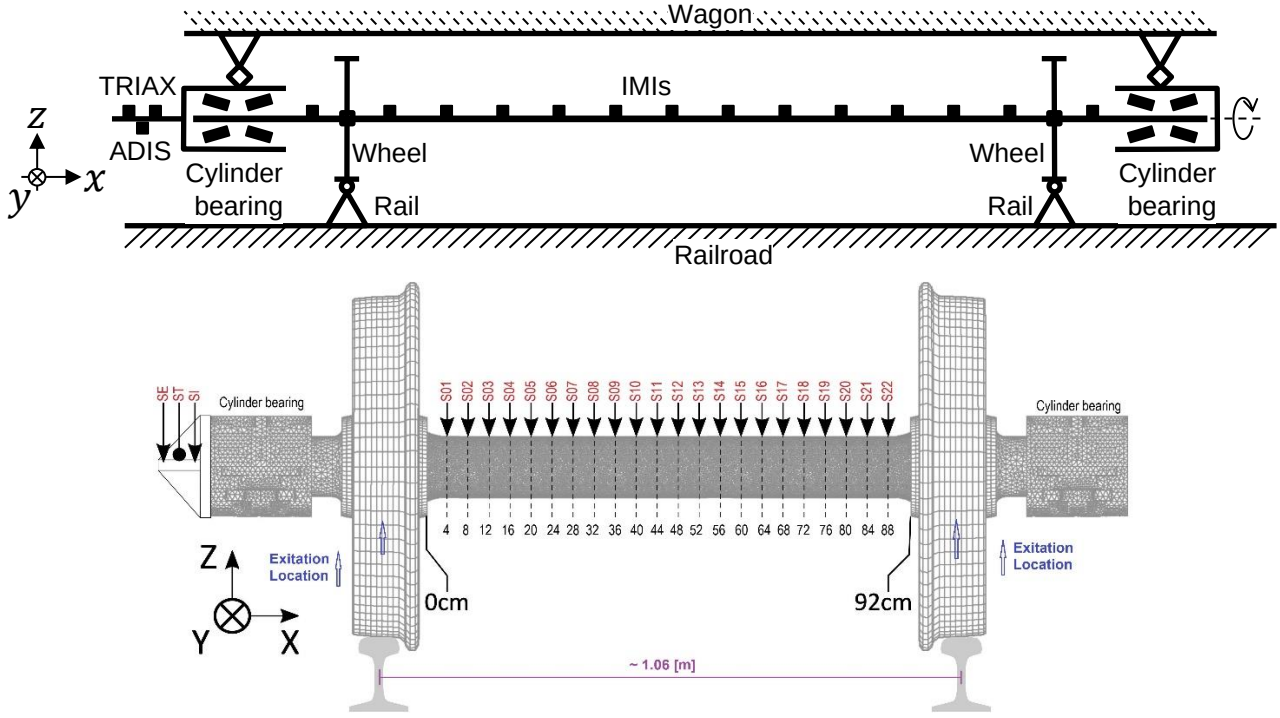

Figure 3.2: Top: Schematic drawing of the axel with different sensors, Bottom: FEM model used for the simulations and location of the virtual sensors (red names) and excitation locations (blue arrows).

3.2 Simulations

The simulations were performed with ADINA 9.6.0. A force of 1000[N] peak of 150[uS] duration in a shape of a half sin period is applied in z direction on a single knot, and the virtual sensors are sampled at 15[uS] (Fs=66,6[Hz]). Figure 3.3 represents the applied force, as well as the accelerations delivered by the two extremes sensors S01 and S22 of Fig.3.2 bottom. On the Fig.3.3. bottom we observe the right most sensor (S22) over 10[mS], there we can recognise an amplitude modulation and decay of several modes.

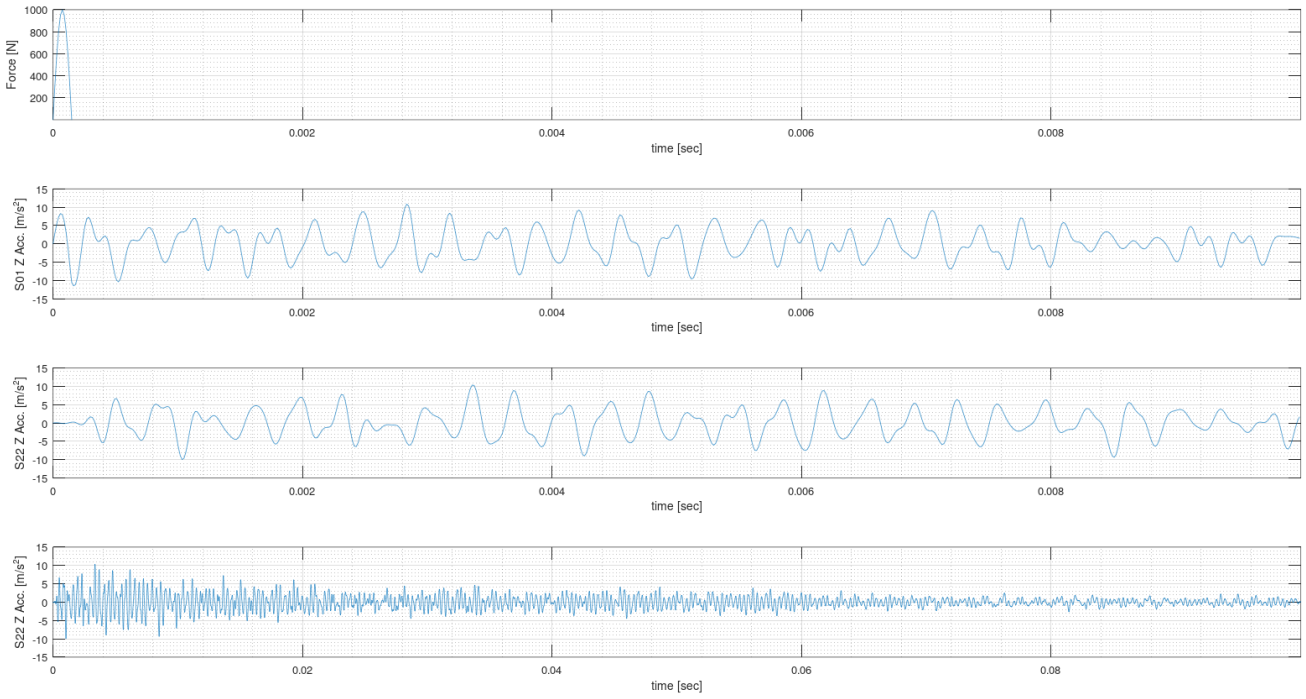

Figure 3.3: From top to bottom: applied force on the left side (near S01), z acceleration of the left most sensor S01, acceleration of the right most sensor S22, and amplitude modulation and decay of S22.

A few examples of axis shapes are represented in Fig.3.4.

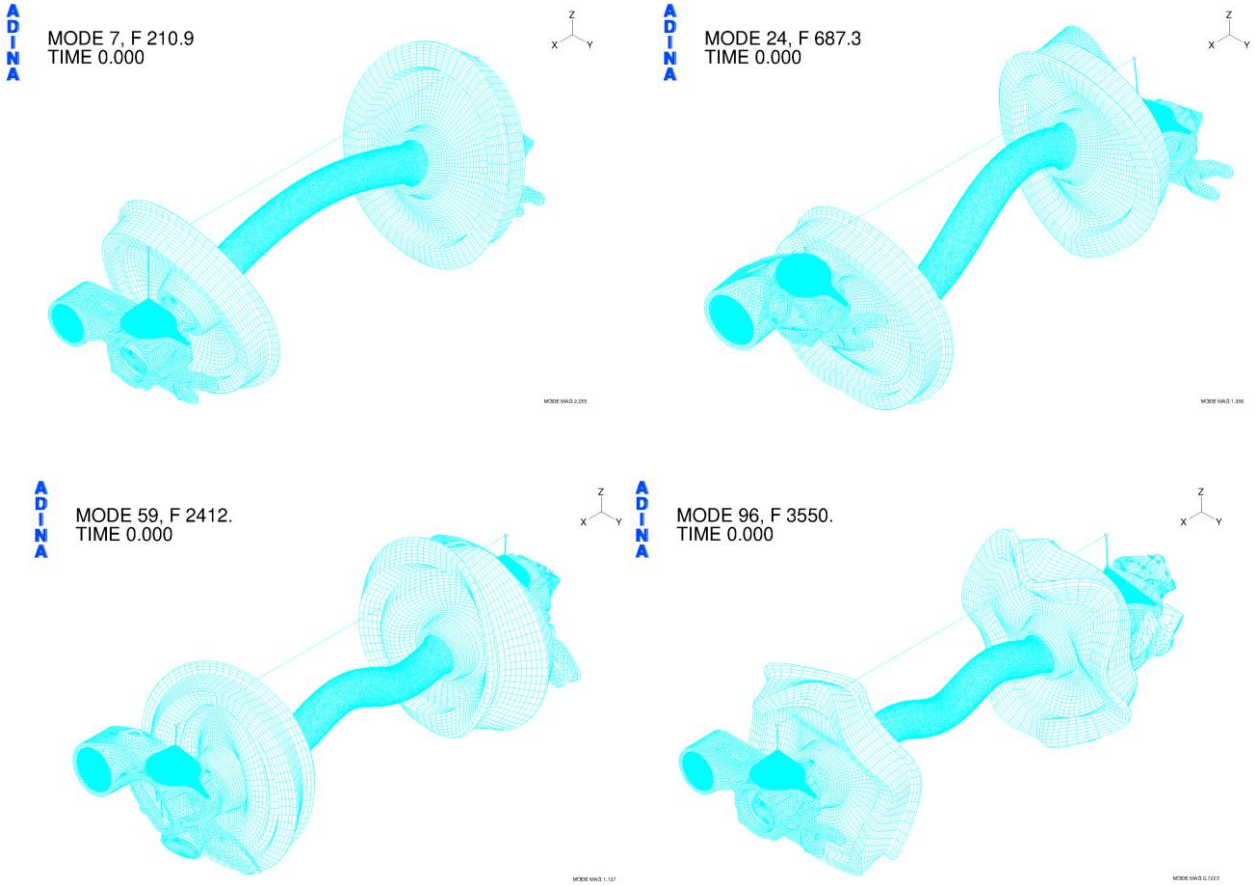

Figure 3.4: Axis and wheel shapes for different transverse modes.

4. STKD applied on the simulations

STKD can be advantageously applied to the mechanical vibrations described above. The important aspect is to separate the extraction done in each dimension to estimate, for each, the analysis dimension (order of ODEs of eq.10), the allowed truncation and the sensors/timespan to consider (boundary effects may have tremendous effects as it will be shown later).

4.1 First space-time dataset reduction

First, we create a matric containing the input dataset obtained from the simulations, in this case the Z accelerations delivered by the virtual sensors. In (10) we use T equidistant time samples and X equidistant sensors; t, x representing the respective sample index. In the example below we used T=2^{12} and X=20, this choice it defined by the number of available sensors (we used S02 to S21) and the natural time constant of the system which appears to be about 1mS including roughly 2^{10} samples. Note that in both cases we avoided border effects by excluding S01 and S22 It improves the "fit" as well by slightly shift the time signal to avoid the part where the oscillation increase, but we lose also some spatial information source (we do not have so much). Indeed, the HODMD shows some issues during those initial transient phase as we will show later, this is an open issue needed to be solved to analyse abrupt transients appearing in real systems subjected to punctual excitations.
The dataset matrix is finally given by Eq. (10):

$$\mathbf{V} = \begin{bmatrix} y_t^x & y_{t+1}^x & \cdots & y_{t+T-1}^x & y_{t+T}^x \\ y_t^{x+1} & y_{t+1}^{x+1} & \cdots & y_{t+T-1}^{x+1} & y_{t+T}^{x+1} \\ \cdots & \cdots & \cdots & \cdots & \cdots \\ y_t^{x+X-1} & y_{t+1}^{x+X-1} & \cdots & y_{t+T-1}^{x+X-1} & y_{t+T}^{x+X-1} \\ y_t^{x+X} & y_{t+1}^{x+X} & \cdots & y_{t+T-1}^{x+X} & y_{t+T}^{x+X} \end{bmatrix} \quad (11)$$

The first operation done is to analyse the "intrinsic dimension" of the dataset by a SVD and singular value representation. The truncation is done manually as the optimal [10] fails to recognise a clear noise floor (to overcome this situation more sensors or a noise floor reference other than the median of the sigma's values are needed). For this case we limit ourself to the first 15 singular values, after a plateau seems to appear.

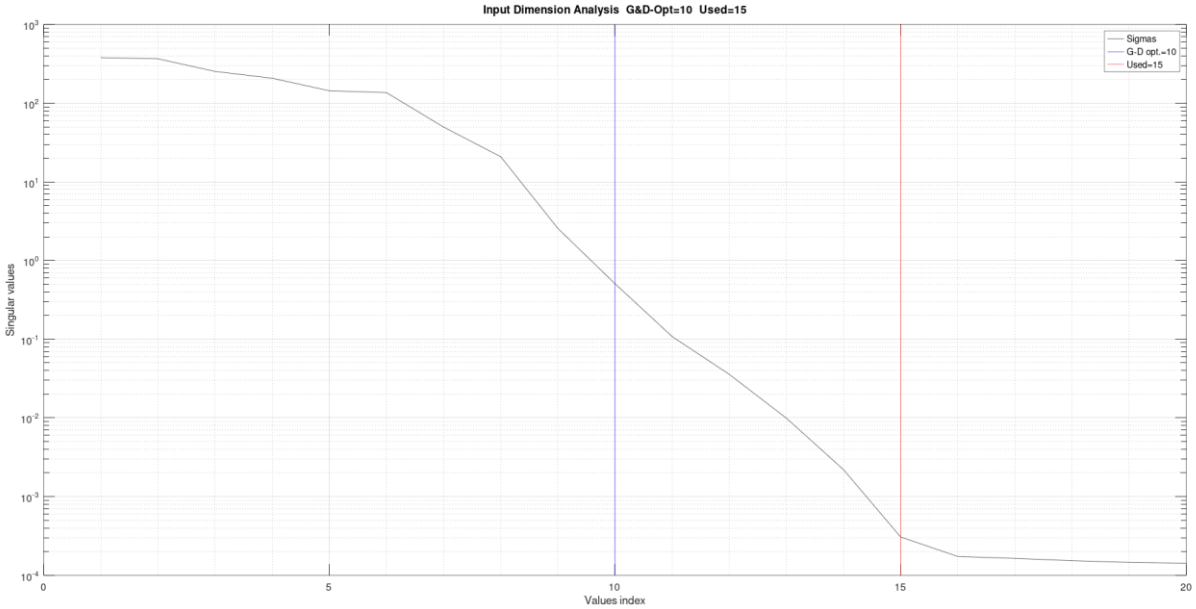

Figure 4.1: From top to bottom: applied force on the left side (near S01), z acceleration of the left most sensor S01, acceleration of the right most sensor S22, and amplitude modulation and decay of S22.

4.2 HODMD on time and space dimension

Based on this truncation, both reduced snapshot matrices $\widehat{\boldsymbol{X}_{nr}}$ and $\widehat{\boldsymbol{T}_{rk}}$ are calculated, and a HODMD analysis is performed. For both cases, the procedure parameters and the obtained relative errors are given in Tab.4.1. Note that several trials were performed concerning the spatial dimension to use. It finally points outs that the mechanical modes are best described by an order 2 ODE, by using higher order it seems we are overfitting.

Parameter	Space	Time
Analysis dimension	2	1000
Dimension truncation	18	Optimum [10]
Amplitude truncation	None (max)	None (max)
Relative Error RMS	2.153E-03	1.872E-06
Relative Error MAX	6.460E-03	2.277E-06

Table 4.1: Used HODMD parameters and fit relative errors

The singular values obtained by those decompositions are depicted in Fig.4.2 and Fig.4.4 for time and space respectively. We may observe that for the time domain, the decomposition of the modified snapshot matrix (left) shows a verry good separation between the relevant content and the noise floor, making it simple to truncate using the optimal approach described in [10]. The amplitude truncation is trickier and the reconstruction error may increase rapidly, so in case of doubts, start with untruncated if calculation time is not a killer criterium. A truncation can still be performed after the whole reconstruction of the signal (space and time). We are going to address this SVD-truncation topic in a next paper. Finally, we extracted 324 singular values in the time domain with this approach. Remembering that those are complex in the case of oscillations (most of them are), and we will obtain ≤ 162 oscillating modes.

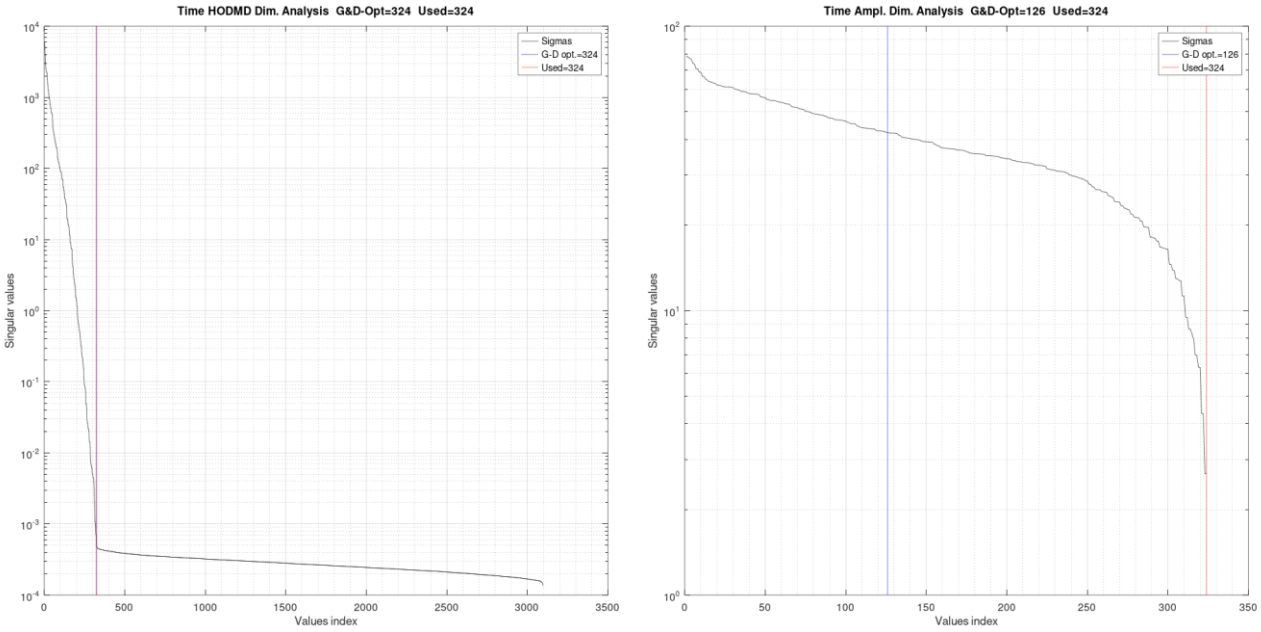

Figure 4.2: SVD and truncation of time HODMD, left: on modified snapshot matrix, right: on amplitude distribution.

Extracted amplitudes and growth rates vs. frequency are represented in Fig. 4.3. (note that the nice shape on the bottom reduce to a linear one in a log-log plot, probably a consequence of the used Lehr's damping model).

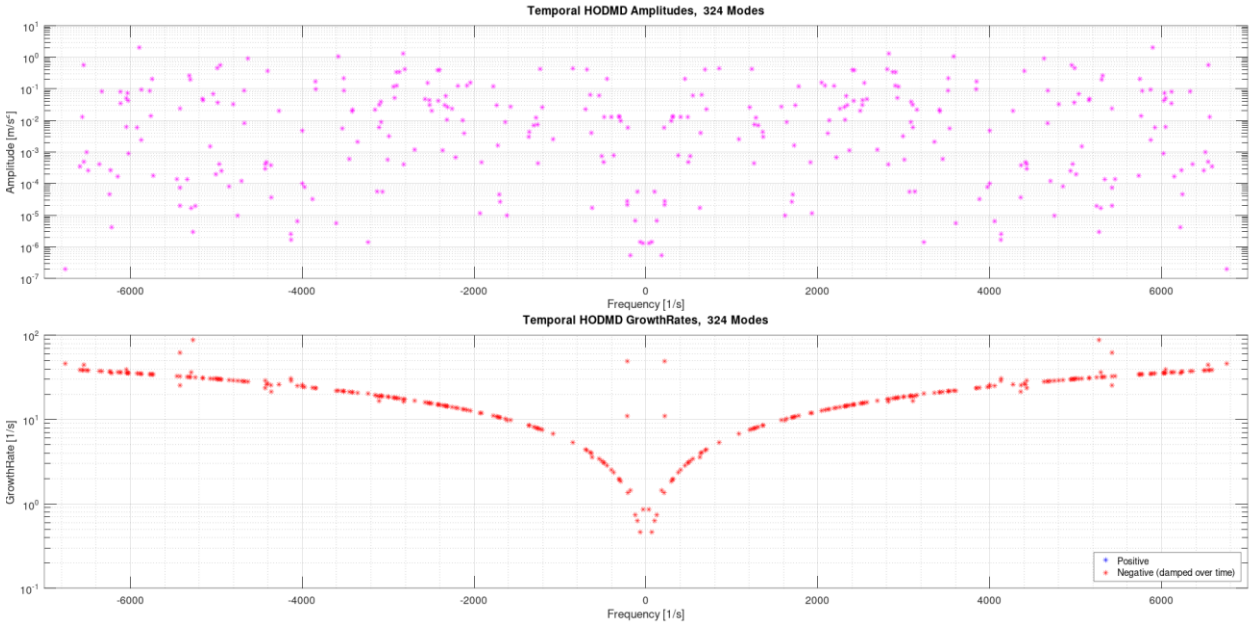

Figure 4.3: Amplitudes (top) and growth rates (bottom) for temporal modes (324 modes and 162 oscillators)

HODMD applied on the spatial dimension is less straightforward due to the limited number of used virtual sensors. As seen on Fig.4.4. left, the decomposition of the modified snapshot matrix has not reached a noise floor as observed for the time domain, making it impossible to obtain an optimal truncation and a whole modal description (we should have taken advantage of the simulation possibilities to extract a larger dataset). Moreover, for each supplemental spatial ODE dimension we use, we "loose" a sensor, therefore a spatial information. Nevertheless, starting with the available dataset we were able to perform a suitable first extraction. As for the time domain, we did not truncate the amplitude

decomposition (Fig.4.4. right) at this stage due to the strong reconstruction error increase. Finally, with 18 extracted singular values, we may expect a maximum of 9 mechanical oscillation modes.

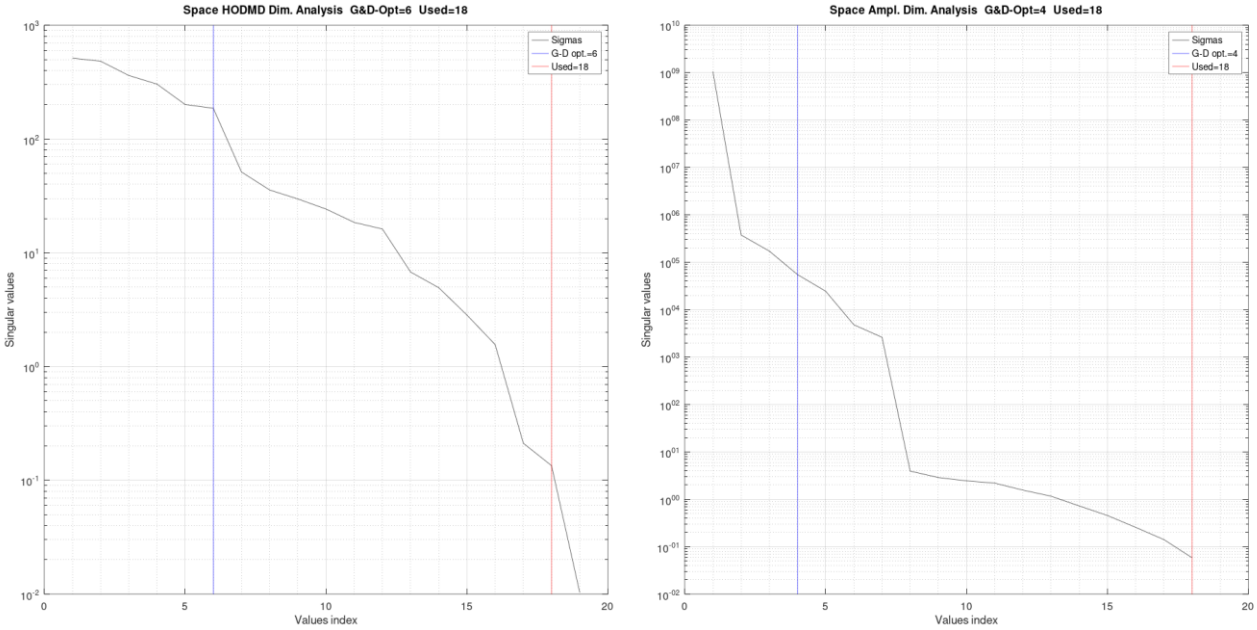

Figure 4.4: SVD and truncation of space HODMD, left: on modified snapshot matrix, right: on amplitude distribution

Extracted amplitudes and growth rates vs. wavenumbers are represented in Fig. 4.5. We obtain 7 oscillator modes (symmetric wavenumbers), 3 pure damping mode (at wavenumber=0) and a single mode which at wavenumber of 12.5 m^{-1} corresponds to a zero wavenumber (sampling theorem, $12.5 = 1/(2 * 0.04)$ for 0.04[m] sensor separation).

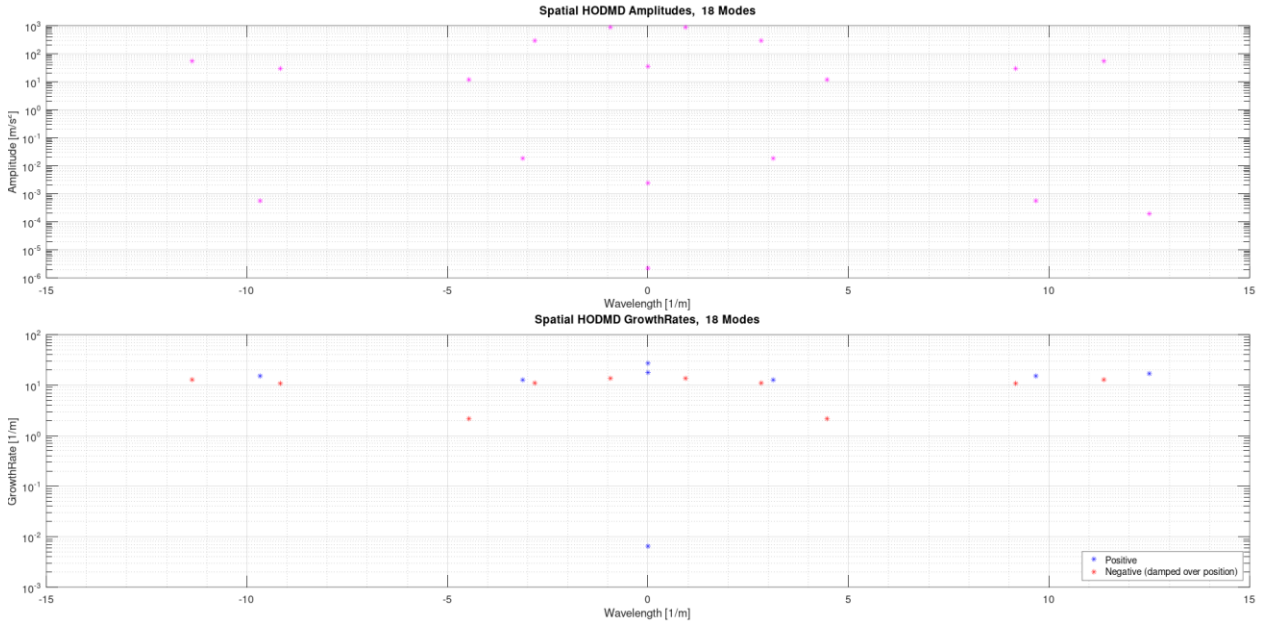

Figure 4.5: Amplitudes (top) and growth rates (bottom) for spatial modes (18 modes and 7 oscillators)

The relative errors are resumed in Tab.4.1. As mentioned earlier, each dimension should be evaluated independently to minimise the relative errors in each before reconstruct the whole signal.

The best way to represent the extracted modes remains the unit circle pole plots, which are represented for each dimension on Fig.4.6. In time dimension the poles relies quite well on the unit circle. There are damped, of course, but their relative time constant to the oscillation period is small so that there cannot be observed at this scaling (we come back to this point later). The spatial dimension behaves differently, we observe modes which tends to grow, which tends to attenuate, and some not oscillating. As mentioned, the reliability is uncertain in the spatial dimension due to the limited number of virtual sensors.

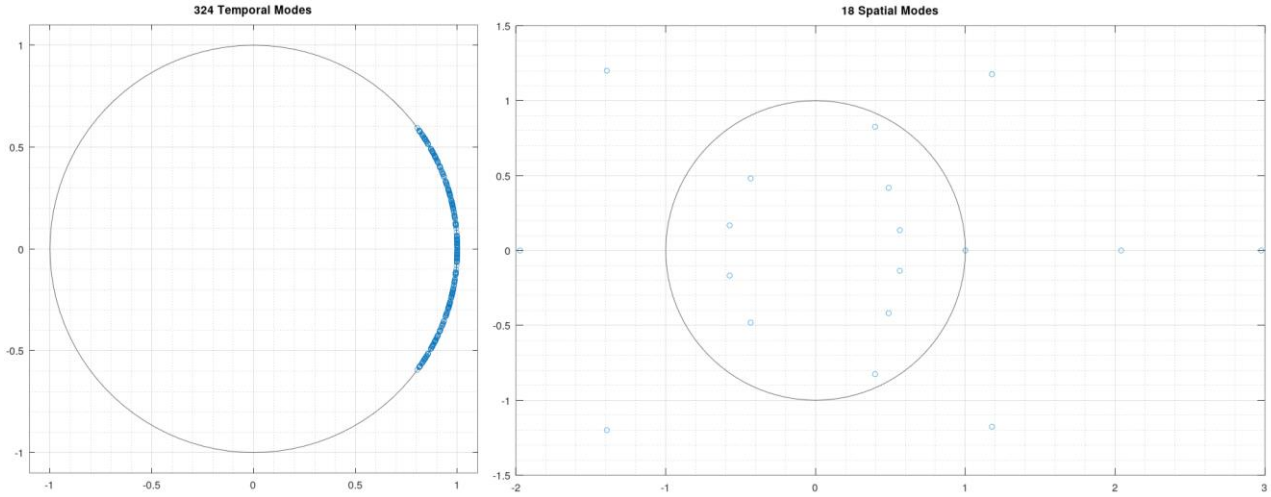

Figure 4.6: Unit circle pole plot for left: time dimension, right: space dimension.

4.3 Reconstruction of the whole spatio-temporal dataset

The modes having been extracted for space and time; the whole spatio-temporal dataset is reconstructed based on Eq. (8). A truncation based on the amplitudes of each component may be envisaged at this point, but as for the HODMD extraction, several analyses showed that this procedure is not blindly recommended.
On Fig. 4.5, the amplitudes of each signal component amplitude as well as the RMS and MAX reconstruction error versus the number of used components are represented. The best solution remains when all are used, even if a local minimum occurs in-between. The formal reason must be analysed in more details.

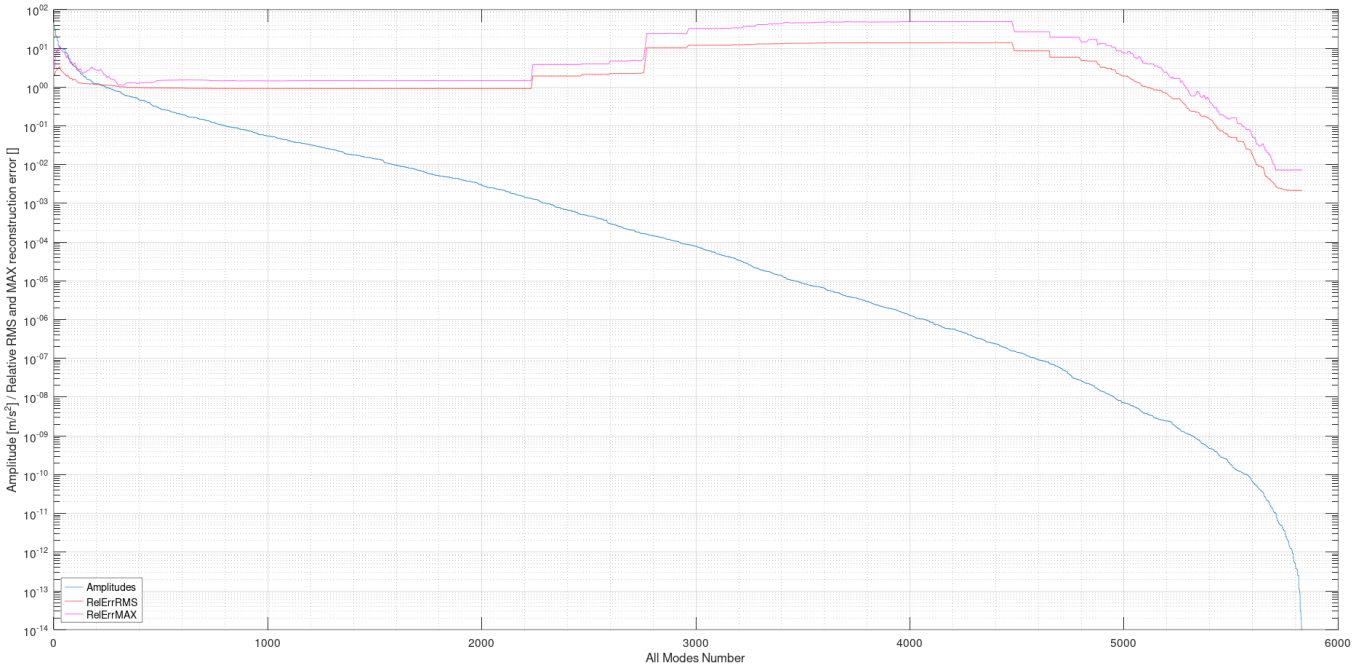

Figure 4.5: Amplitudes of all modes and reconstruction error vs. number of used components

All modes amplitudes versus extracted frequencies and wavenumbers as well as the dispersion diagram are represented on Fig. 4.6. A clear distinction between 14 spatial modes can be observed (vertical lines on the top-right graphic, giving 7 oscillation mods), whereas in the time domain (bottom left graphic) only a more fainted structure in form of vertical lines can be recognised (324 symmetric temporal modes where extracted, see fig. 4.2., leading to 162 oscillation modes).

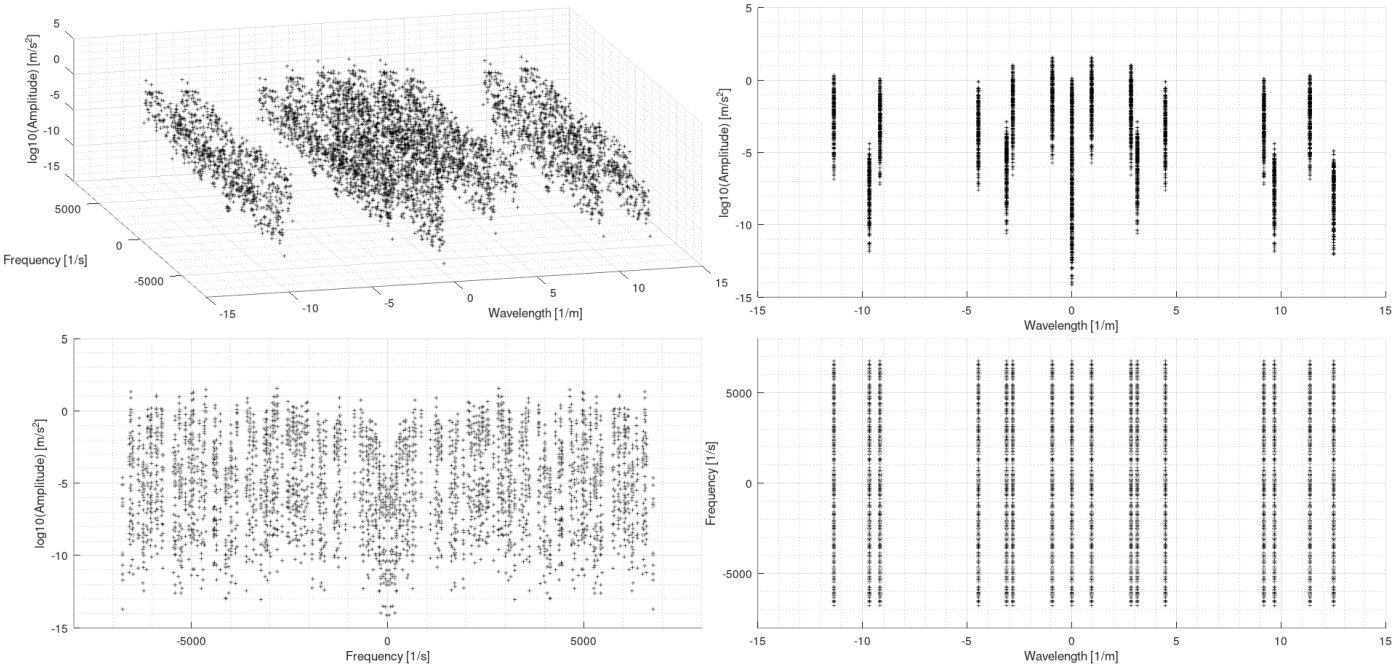

Figure 4.6: Z acceleration dispersion diagram with amplitude and projections.

As an example, the original signal and the reconstruction along time for several sensors and along space at different time snapshots are depicted on figure 4.7. This representation is, of course, subjective, but the overall good fit confirms the small errors.

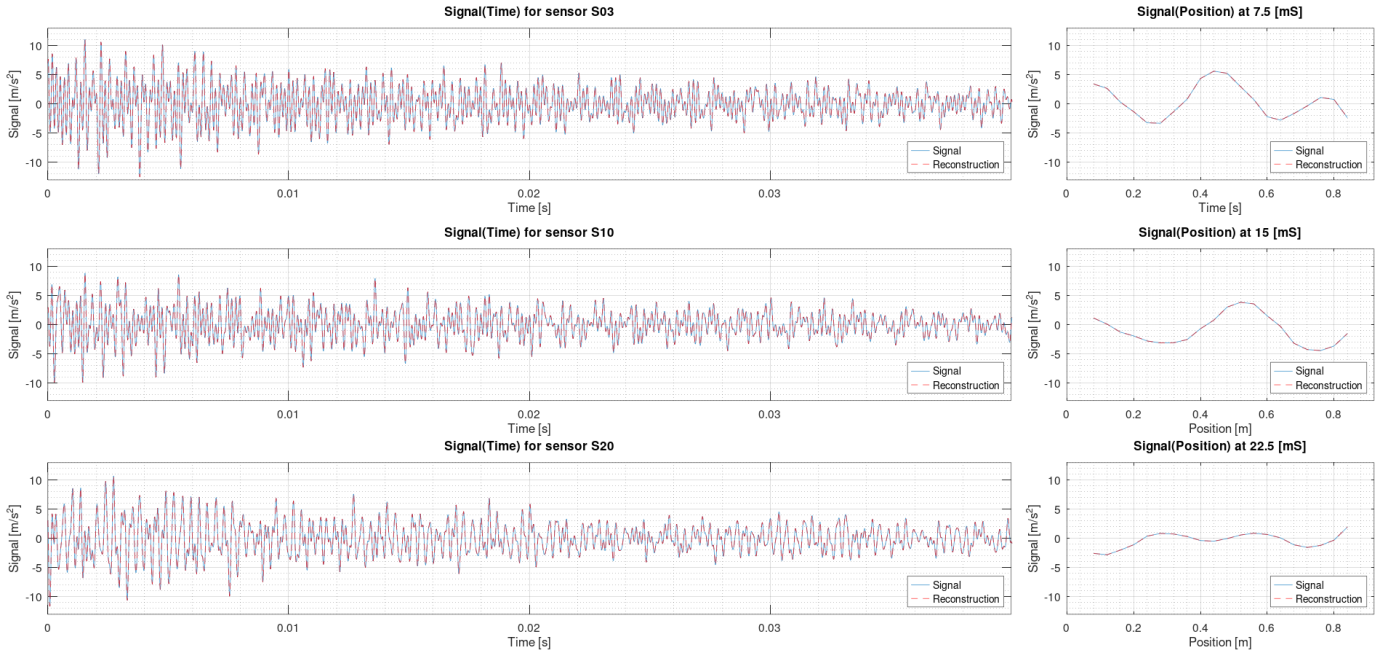

Figure 4.7: Z acceleration simulated and reconstructed signals over time for different sensors and over space for different timestamps

4.4 Extraction of accelerations, velocities, and positions

Previously we described the extractions on the simulated z acceleration as example. This comes from the consideration that measurements are generally performed with the help of accelerometers mounted on the mechanical structures. Considering the possibility to easily extract the velocities and the positions from the simulations or by optical means, it is worth to perform this analysis from them as well. The simulation data has been compiled to a film representing the evolution of the vibration over time, and **Fig.4.8** shows a snapshot of it. Note that more virtual sensors as depicted in **Fig.3.2** have been used, but we will not focus on them in this analysis.

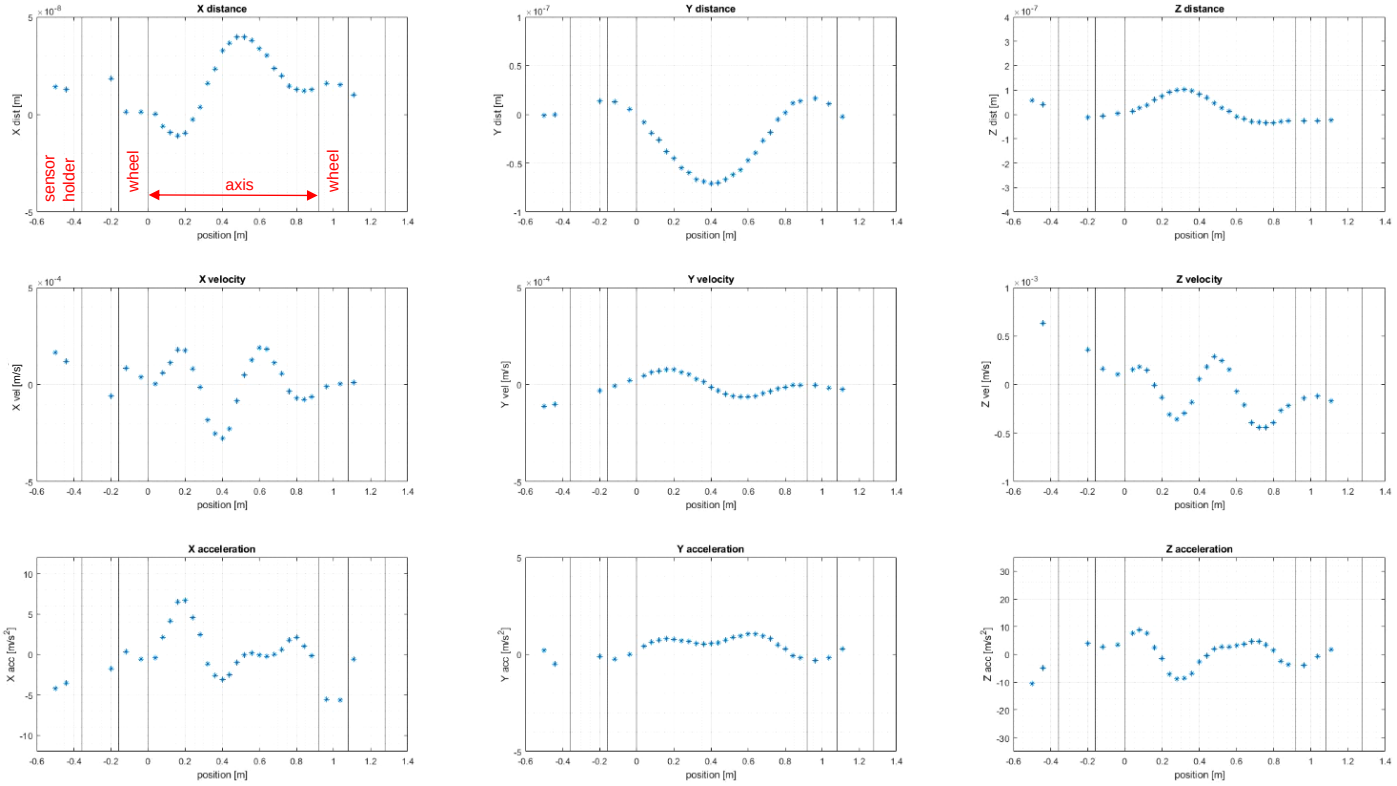

Figure 4.8: Simulated position, velocity, and acceleration for all virtual sensors (timestamp).

Applying this extraction procedures on acceleration, velocities and positions, lead to verry similar results with the smallest errors for the positions (derivative calculations in ADINA?). Those results are resumed in the 2D colour plots over time and space of **Figures 4.9 to 4.19**. The extraction parameters, number of modes and errors are resumed in **Tables 4.2. to 4.4**. The main difficulty of this procedure is that a fully automatic approach cannot be implemented yet. To do so, the dimensionality analysis and truncations methodologies should be improved. We may look if SINDy [12] approach can help for the dimensionality analysis.

As we observe, the simulations can be represented verry well with 18 spatial modes (14 oscillators and 4 pure damped modes) and 310 to 350 temporal modes (155-175 oscillators with some few pure damped modes). It is quite remarkable that that such a complex system (vibrating axis, vibrating wheels, loose contact between wheel and railroad) can be braked down from transient simulation to a relative sparce modal description. A further task will be to verify if this procedure can be transferred on acceleration measurements of real systems under operation to finally extract their modes and evolution over time to monitor ageing for preventive maintenance.

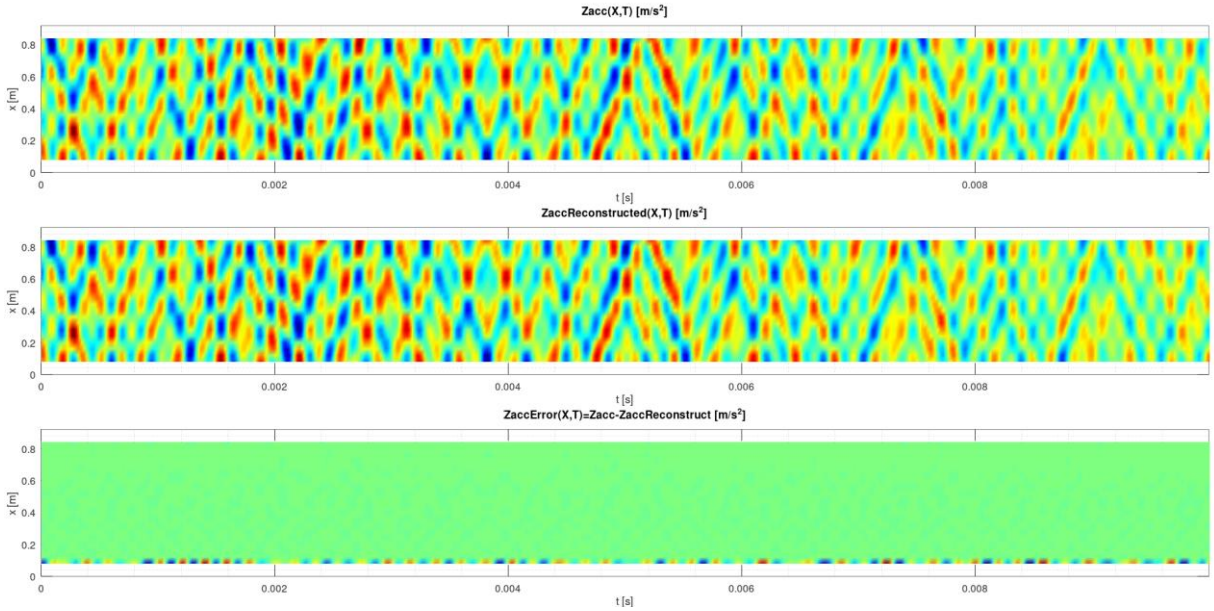

Figure 4.9: Z acceleration simulated, reconstructed and error over space and time

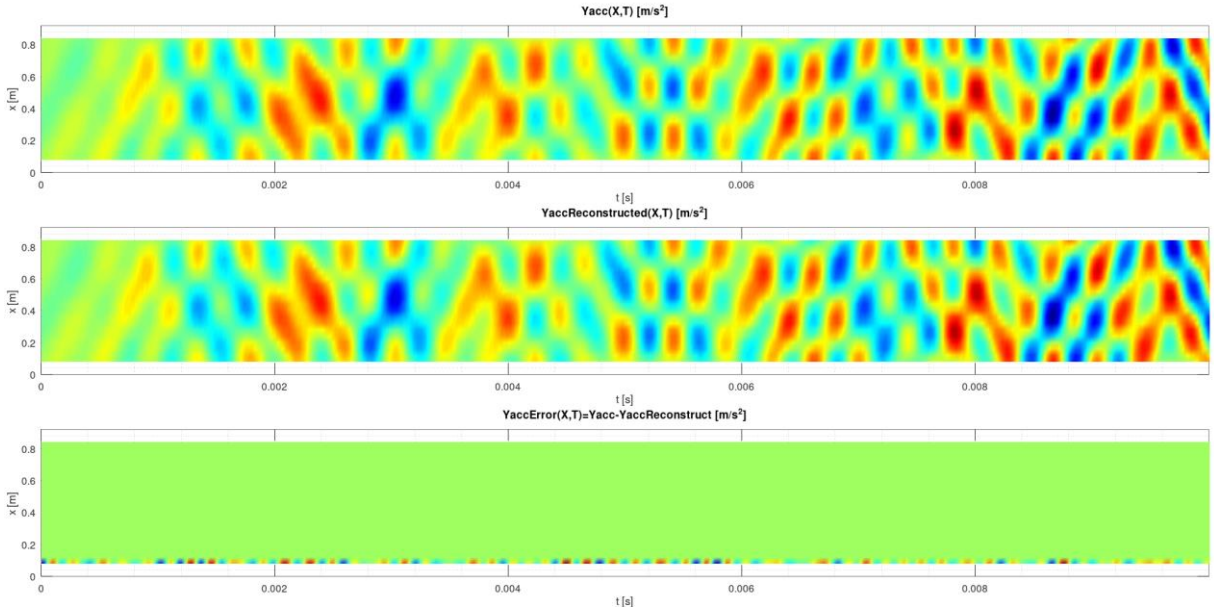

Figure 4.10: Y acceleration simulated, reconstructed and error over space and time

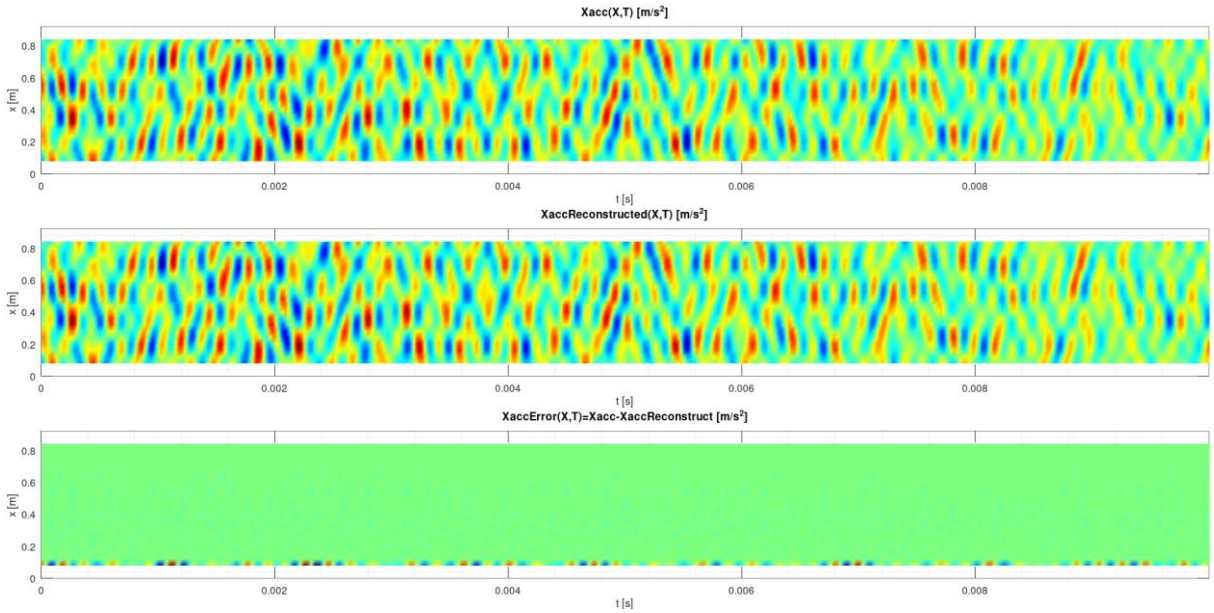

Figure 4.11: X acceleration simulated, reconstructed and error over space and time

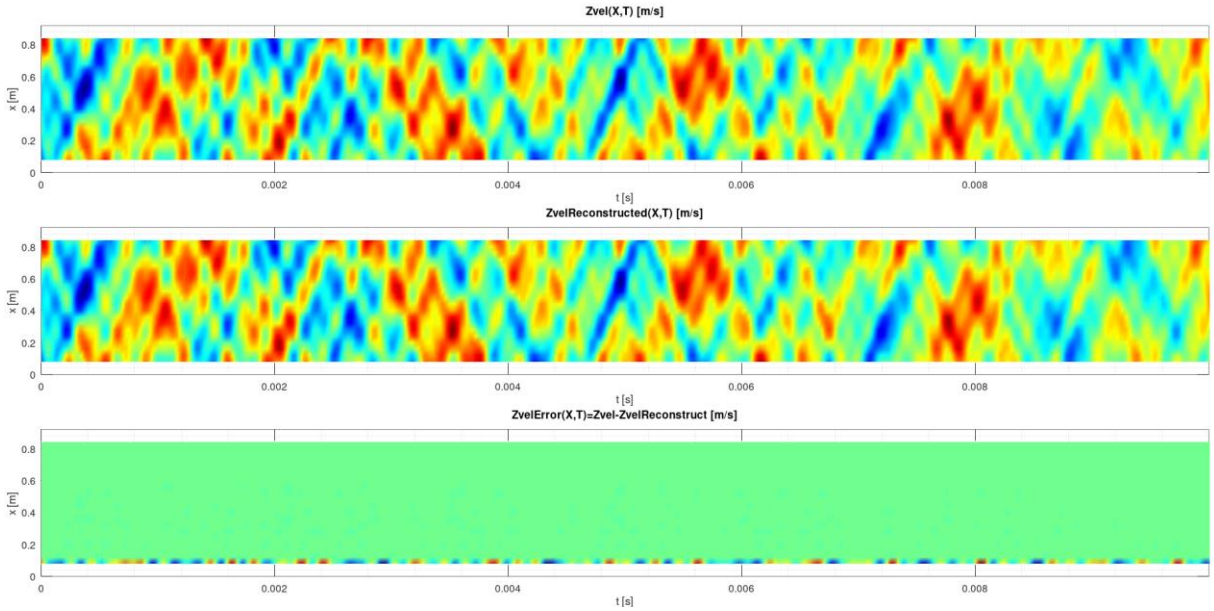

Figure 4.12: Z velocity simulated, reconstructed and error over space and time

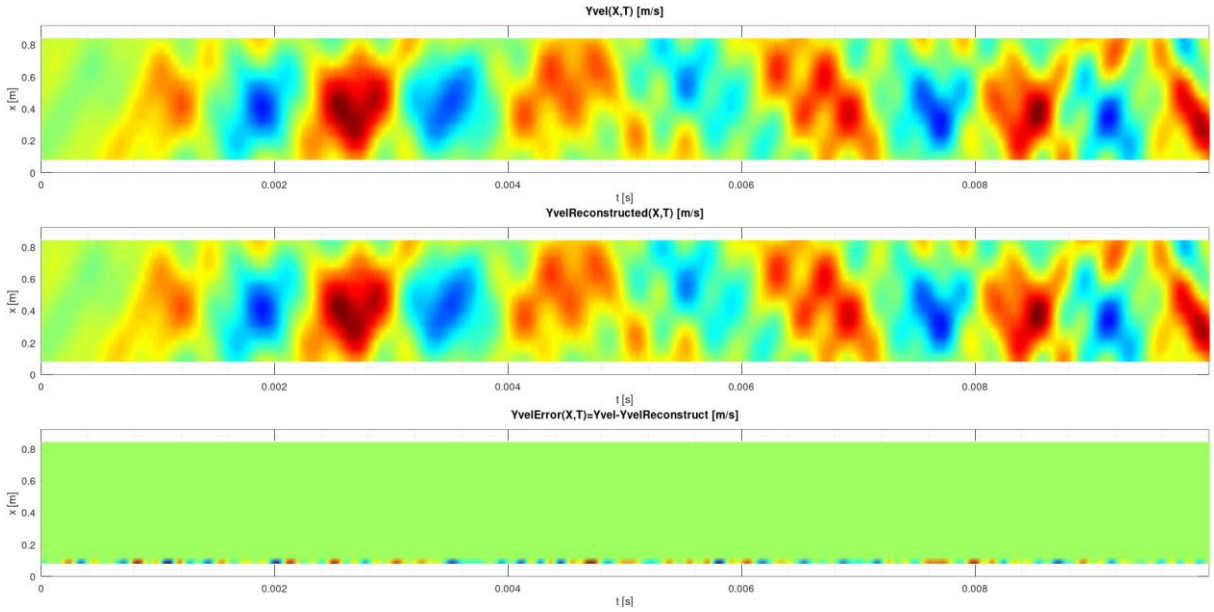

Figure 4.13: Y velocity simulated, reconstructed and error over space and time

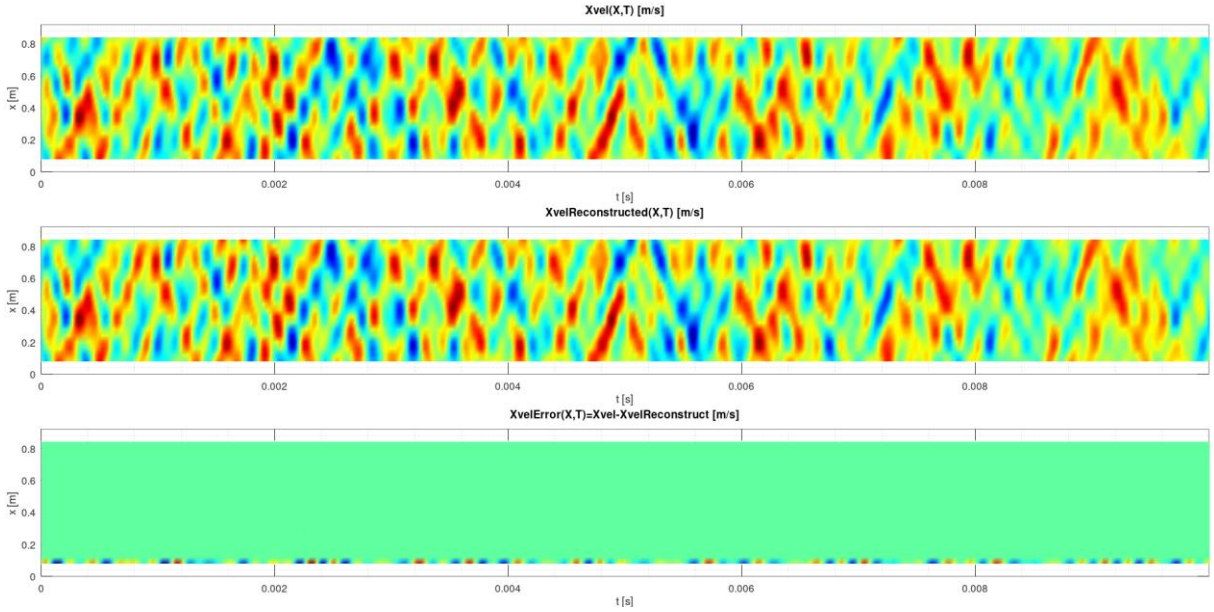

Figure 4.14: X velocity simulated, reconstructed and error over space and time

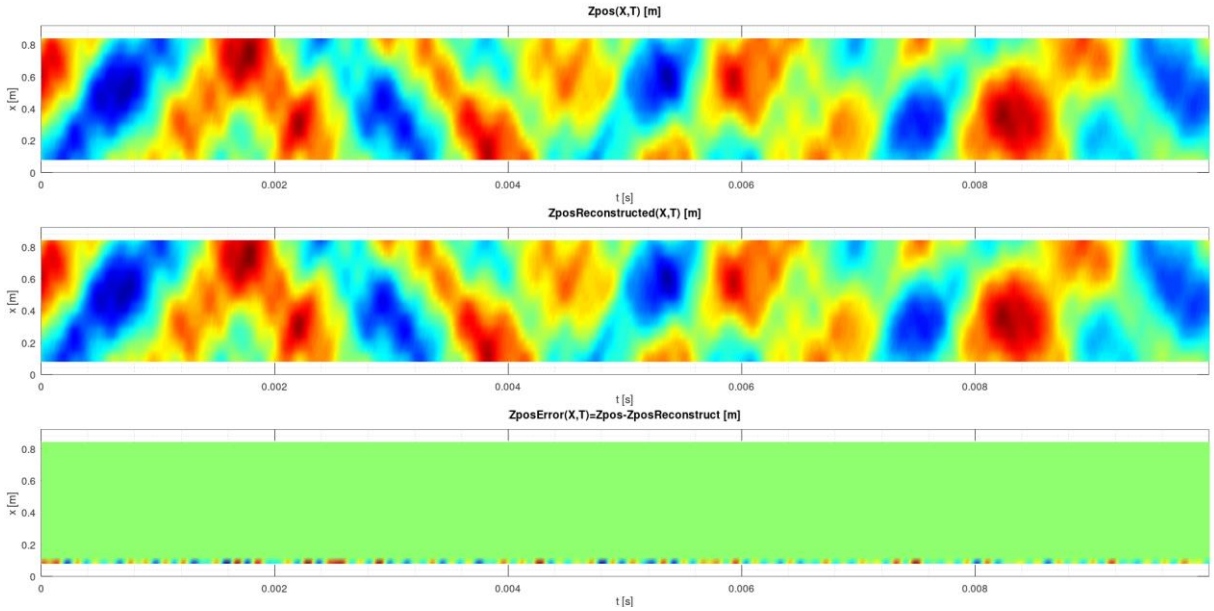

Figure 4.15: Z displacement simulated, reconstructed and error over space and time

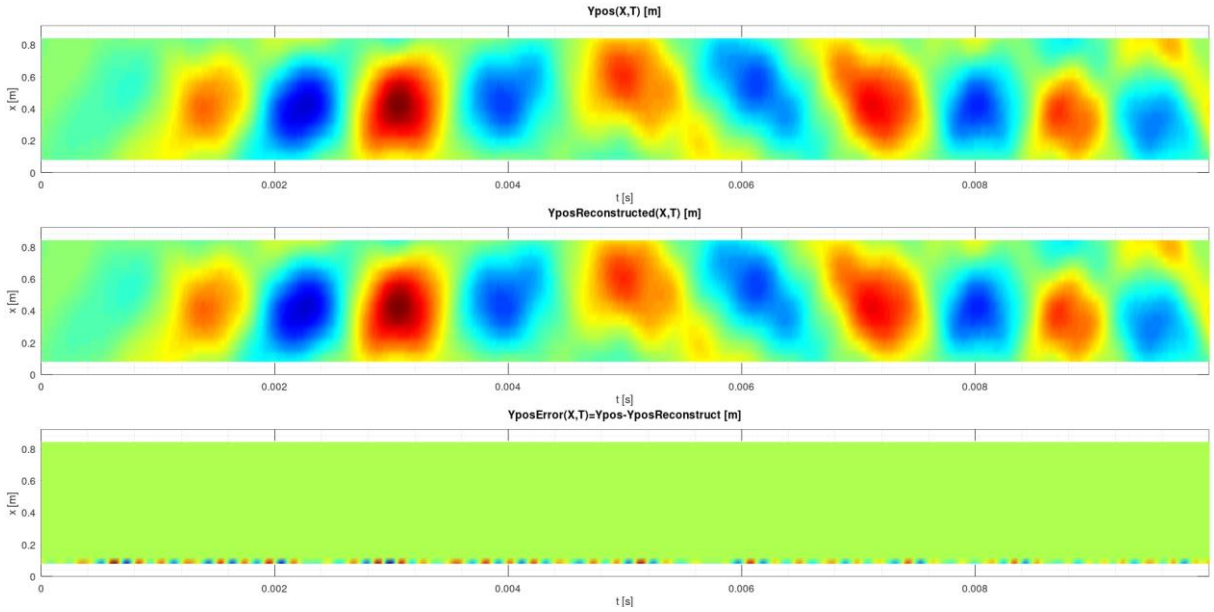

Figure 4.16: Y displacement simulated, reconstructed and error over space and time

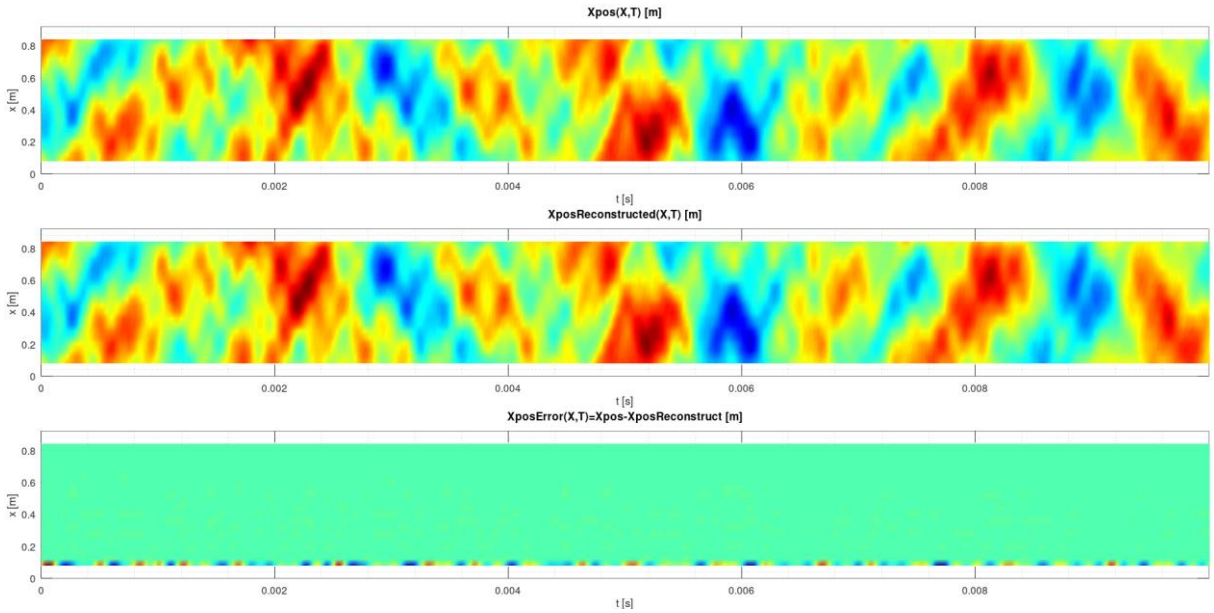

Figure 4.17: X displacement simulated, reconstructed and error over space and time

Extraction Results	Z acceleration		Y acceleration		X acceleration	
Parameters / Dimension	**Space**	**Time**	**Space**	**Time**	**Space**	**Time**
Dataset size	20	4096	20	4096	20	4096
Input single value truncation	15		17		15	
Analysis dimension	2	1000	2	1000	2	1000
Dimension truncation	18	Optimum [10]	18	350	18	Optimum [10]
Amplitude truncation	None (max)	None (max)	None (max)	None (max)	None (max)	None (max)
Numbr of used singular values	18	324	18	350	18	328
Relative Error RMS	2.153E-03	1.872E-06	3.715E-04	3.526E-06	2.673E-03	4.873E-06
Relative Error MAX	6.460E-03	2.277E-06	7.914E-04	5.349E-06	1.167E-02	2.899E-06
Numbrer of total modes	5832 (18x324)		6300 (18x350)		5904 (18x328)	
Amplitude truncation	None (max)		None (max)		None (max)	
Combined Relative Error RMS	2.149E-03		3.760E-04		2.681E-03	
Combined Relative Error MAX	7.283E-03		1.430E-03		9.897E-03	
Max. number of oscillators	1458 (9x162)		1575 (9x175)		1476 (9x164)	

Table 4.2: Resume of parameters and errors for Z, Y and X accelerations.

Extraction Results	Z velocity		Y velocity		X velocity	
Parameters / Dimension	**Space**	**Time**	**Space**	**Time**	**Space**	**Time**
Dataset size	20	4096	20	4096	20	4096
Input single value truncation	15		17		15	
Analysis dimension	2	1000	2	1000	2	1000
Dimension truncation	18	Optimum [10]	18	Optimum [10]	18	Optimum [10]
Amplitude truncation	None (max)	None (max)	None (max)	None (max)	None (max)	None (max)
Numbr of used singular values	18	314	18	340	18	320
Relative Error RMS	1.408E-03	2.268E-06	2.576E-04	3.036E-06	2.345E-03	3.420E-06
Relative Error MAX	4.110E-03	3.948E-06	5.439E-04	2.939E-06	1.164E-02	6.083E-06
Numbrer of total modes	5652 (18x324)		6120 (18x340)		5760 (18x320)	
Amplitude truncation	None (max)		None (max)		None (max)	
Combined Relative Error RMS	1.413E-03		2.706E-04		2.344E-03	
Combined Relative Error MAX	5.827E-03		1.216E-03		1.012E-02	
Max. number of oscillators	1413 (9x157)		1530 (9x170)		1440 (9x160)	

Table 4.3: Resume of parameters and errors for Z, Y and X velocities.

Extraction Results	Z position		Y position		X position	
Parameters / Dimension	**Space**	**Time**	**Space**	**Time**	**Space**	**Time**
Dataset size	20	4096	20	4096	20	4096
Input single value truncation	15		17		15	
Analysis dimension	2	1000	2	1000	2	1000
Dimension truncation	18	Optimum [10]	18	Optimum [10]	18	Optimum [10]
Amplitude truncation	None (max)	None (max)	None (max)	None (max)	None (max)	None (max)
Numbr of used singular values	18	311	18	323	18	311
Relative Error RMS	6.276E-04	1.522E-06	1.304E-04	2.041E-06	7.680E-04	2.316E-06
Relative Error MAX	1.749E-03	2.338E-06	3.063E-04	2.377E-06	2.857E-03	2.574E-06
Numbrer of total modes	5598 (18x311)		5814 (18x323)		5598 (18x311)	
Amplitude truncation	None (max)		None (max)		None (max)	
Combined Relative Error RMS	6.267E-04		1.730E-04		7.687E-04	
Combined Relative Error MAX	3.961E-03		1.383E-03		4.715E-03	
Max. number of oscillators	1395 (9x155)		1449 (9x161)		1395 (9x155)	

Table 4.4: Resume of parameters and errors for Z, Y and X positions.

4.5. HODMD issues

There are some important points to take into consideration when applying HODMD to a dataset. As we can see on Fig. 4.9 to 4.17, the error is highest at the sensor nearest from the excitation point, and the first most sensor (S01) has been excluded for this reason. A similar procedure has been applied to the time domain, the initial samples where the signal increase (just during and after the excitation) has been excluded from the extraction. As FFT shows some issues when the amplitude is not constant (or varies slowly), so the HODMD can show some issues when the signal amplitude is not exponentially monotonous. In some way this can be correlated with non-normal systems (degenerated or quasi-degenerated modes where ODE solutions are given by $t^n e^{(\delta+j\omega)t}$ n being the order of degeneracy). This will not be accessed in this paper; we will try to cover it on a separated one dedicated to the HODMD and truncation of signals obtained from real mechanical systems submitted to sporadic excitation (as produced by railroad on a wheel during operation).

5. Analysis

Extracted frequencies, wavenumbers and growth rates in space and time are looked over hereafter. As the spatial dimension is much lower and easier to overview, we start with it before accessing the temporal one.

5.1 Spatial results

Given the limited spatial dimension (only 20 sensors and 18 modes were used, respectively extracted) the analysis can be performed manually. Those wavenumbers, growthrates and amplitudes (HODMD of $\widehat{X_{nr}}$, not after recombination with spatial analysis) are resumed in **Tables 5.1, to 5.3**.

Extracted spatial wavenumber [m^{-1}] for								
x Displacement	y Displacement	z Displacement	x Velocity	y Velocity	z Velocity	x Acceleration	y Acceleration	z Acceleration
-11.452	-11.507	-11.435	-11.424	-11.404	-11.380	-11.410	-11.389	-11.367
-9.812	-9.975	-9.796	-9.773	-9.728	-9.689	-9.766	-9.699	-9.671
-9.310	-9.469	-9.290	-9.278	-9.245	-9.188	-9.263	-9.214	-9.168
-4.388	-4.383	-4.485	-4.389	-4.411	-4.476	-4.407	-4.410	-4.465
-3.032	-3.117	-3.131	-3.034	-3.008	-3.125	-3.072	-3.051	-3.123
-2.720	-2.679	-2.866	-2.729	-2.788	-2.840	-2.760	-2.766	-2.822
-0.908	-0.895	-0.981	-0.905	-0.970	-0.951	-0.935	-0.944	-0.937
0.000	-0.417	0.000	0.000	0.000	0.000	0.000	0.000	0.000
0.000	0.000	0.000	0.000	0.000	0.000	0.000	0.000	0.000
0.000	0.417	0.000	0.000	0.000	0.000	0.000	0.000	0.000
0.908	0.895	0.981	0.905	0.970	0.951	0.935	0.944	0.937
2.720	2.679	2.866	2.729	2.788	2.840	2.760	2.766	2.822
3.032	3.117	3.131	3.034	3.008	3.125	3.072	3.051	3.123
4.388	4.383	4.485	4.389	4.411	4.476	4.407	4.410	4.465
9.310	9.469	9.290	9.278	9.245	9.188	9.263	9.214	9.168
9.812	9.975	9.796	9.773	9.728	9.689	9.766	9.699	9.671
11.452	11.507	11.435	11.424	11.404	11.380	11.410	11.389	11.367
12.500	12.500	12.500	12.500	12.500	12.500	12.500	12.500	12.500

Table 5.1: Extracted wavenumbers on displacements, velocities, and accelerations.

Extracted spatial growthrates [m^{-1}] for								
x Displacement	y Displacement	z Displacement	x Velocity	y Velocity	z Velocity	x Acceleration	y Acceleration	z Acceleration
-14.6990	-16.4570	-14.1530	-14.3370	-13.7820	-13.0130	-14.0710	-13.2520	-12.8840
16.7720	18.3110	16.2180	16.5470	16.3690	15.4180	16.3770	16.0740	15.2340
-11.7270	-12.9410	-11.4830	-11.6390	-11.3130	-10.8870	-11.5440	-10.9040	-10.8720
-2.1693	-1.9921	-2.2141	-2.1991	-2.1744	-2.1196	-2.1640	-1.8908	-2.1710
14.1300	15.3820	13.3570	13.8330	13.3610	12.8800	13.7460	13.6740	12.7430
-12.0670	-12.7720	-11.4050	-11.9700	-11.7430	-10.9910	-11.8280	-11.371	-11.0500
-15.1130	-16.0590	-13.6580	-14.9870	-14.1360	-13.5060	-14.5790	-14.011	-13.6810
0.0003	23.8270	0.0026	0.0016	0.0078	0.0036	0.0069	0.0017	0.0065
19.6880	0.0004	19.2010	18.7530	17.5510	18.2440	18.9350	19.0570	17.8280
29.0210	23.8270	26.5140	30.3370	33.5790	26.8510	28.6750	28.5080	27.2640
-15.1130	-16.0590	-13.6580	-14.9870	-14.1360	-13.5060	-14.5790	-14.011	-13.6810
-12.0670	-12.7720	-11.4050	-11.9700	-11.7430	-10.9910	-11.8280	-11.371	-11.0500
14.1300	15.3820	13.3570	13.8330	13.3610	12.8800	13.7460	13.6740	12.7430
-2.1693	-1.9921	-2.2141	-2.1991	-2.1744	-2.1196	-2.1640	-1.8908	-2.1710
-11.7270	-12.9410	-11.4830	-11.6390	-11.3130	-10.8870	-11.5440	-10.9040	-10.8720
16.7720	18.3110	16.2180	16.5470	16.3690	15.4180	16.3770	16.0740	15.2340
-14.6990	-16.4570	-14.1530	-14.3370	-13.7820	-13.0130	-14.0710	-13.2520	-12.8840
19.4790	21.7970	18.7090	18.9620	18.4920	17.2790	18.7050	17.9680	17.0020

Table 5.2: Extracted growthrates on displacements, velocities, and accelerations (1:1 correspondence to tab.5.1).

Extracted spatial amplitudes, diplacements in [m], velocities in [m/s], accelerations in [m/s^2] for								
x Displacement	y Displacement	z Displacement	x Velocity	y Velocity	z Velocity	x Acceleration	y Acceleration	z Acceleration
2.45E-07	4.08E-07	6.20E-07	2.54E-03	1.06E-03	3.23E-03	6.57E+01	1.15E+01	5.40E+01
5.14E-13	2.86E-13	1.83E-12	7.30E-09	3.38E-09	2.14E-08	1.92E-04	4.17E-05	5.64E-04
7.81E-08	1.12E-07	1.97E-07	1.13E-03	3.88E-04	1.38E-03	3.33E+01	4.56E+00	2.93E+01
1.98E-08	1.82E-08	5.34E-08	3.03E-04	1.11E-04	4.67E-04	8.94E+00	1.29E+00	1.18E+01
1.65E-11	9.08E-12	6.45E-11	2.43E-07	1.36E-07	6.95E-07	5.99E-03	1.28E-03	1.84E-02
8.63E-07	1.01E-06	1.82E-06	1.16E-02	4.36E-03	1.41E-02	3.27E+02	5.37E+01	2.89E+02
3.42E-06	4.19E-06	7.21E-06	3.77E-02	1.53E-02	4.98E-02	9.58E+02	1.88E+02	8.72E+02
2.77E-07	2.38E-13	7.78E-07	1.56E-03	1.76E-03	3.31E-03	2.76E+01	8.98E+00	3.50E+01
2.06E-12	4.96E-07	8.83E-12	3.74E-08	3.24E-08	9.57E-08	8.23E-04	1.58E-04	2.43E-03
1.83E-15	2.38E-13	3.59E-14	6.17E-12	1.72E-13	1.53E-10	5.54E-07	1.32E-07	2.23E-06
3.42E-06	4.19E-06	7.21E-06	3.77E-02	1.53E-02	4.98E-02	9.58E+02	1.88E+02	8.72E+02
8.63E-07	1.01E-06	1.82E-06	1.16E-02	4.36E-03	1.41E-02	3.27E+02	5.37E+01	2.89E+02
1.65E-11	9.08E-12	6.45E-11	2.43E-07	1.36E-07	6.95E-07	5.99E-03	1.28E-03	1.84E-02
1.98E-08	1.82E-08	5.34E-08	3.03E-04	1.11E-04	4.67E-04	8.94E+00	1.29E+00	1.18E+01
7.81E-08	1.12E-07	1.97E-07	1.13E-03	3.88E-04	1.38E-03	3.33E+01	4.56E+00	2.93E+01
5.14E-13	2.86E-13	1.83E-12	7.30E-09	3.38E-09	2.14E-08	1.92E-04	4.17E-05	5.64E-04
2.45E-07	4.08E-07	6.20E-07	2.54E-03	1.06E-03	3.23E-03	6.57E+01	1.15E+01	5.40E+01
1.33E-13	4.84E-14	5.66E-13	2.11E-09	1.32E-09	8.23E-09	5.58E-05	1.60E-05	1.95E-04

Table 5.3: Extracted amplitudes on displacements, velocities, and accelerations (1:1 correspondence to tab.5.1).

For wavenumbers (table 5.1) we observe complete symmetric pairs of positive and negative values, whereas the growthrates and amplitudes values are identical for each pair (as classical FFT of a real signal except for not extracted growthrates). Note the outlier at the bottom line, it corresponds to a 0 wavenumber (as for FFT of a discrete periodic signal we obtain 2 borders). On rows we observe nearly identical wavenumber, the discrepancies are probably due to the limited spatial resolution and boundary effects. An indicator for those hypotheses is **Fig.4.4**. left, the singular values do not reach the plateau observed in **Fig.4.4.2**. left, some modes are probably missing; the supplemental non-zero mode observed on y displacement column (which seems to perturbate the nearby mode slightly) and the description below (**Fig.5.1**). A conclusion at this point is that we should verify a higher spatial resolution.

On **Table 5.4.** we calculated the wavelength from positive values of **Table.5.1**. and some statistical values. First, we observe on last row that the values correspond exactly to twice the distance of the spatial sampling (4cm), which is coherent with the sampling theorem requiring 2 samples per period. No shorter wave can be observed. Secondly, we observe that the largest wavelength (if we exclude the outlier in the y displacement) corresponds well to the distance between both contact points between rails and wheels (~ 1.06 [m], see **Fig.3.2**.) and the first half mechanical period. All those results tend to confirm the coherence of the extraction.

	Extracted positiv spatial wavelengths [m] and statistics														
	x Disp.	y Disp.	z Disp.	x Vel.	y Vel.	z Vel.	x Acc.	y Acc.	z Acc.	Min	Max	Mean	Sigma	Range	S/M [%]
-	Inf	Inf	Inf	Inf	Inf	Inf	Inf	Inf	Inf	-	-	-	-	-	-
-	Inf	2.398	Inf	Inf	Inf	Inf	Inf	Inf	Inf	-	-	-	-	-	-
Mode 1	1.102	1.117	1.019	1.106	1.031	1.052	1.070	1.060	1.067	1.019	1.117	1.069	0.034	0.098	3.139
Mode 2	0.368	0.373	0.349	0.366	0.359	0.352	0.362	0.362	0.354	0.349	0.373	0.361	0.008	0.024	2.190
Mode 3	0.330	0.321	0.319	0.330	0.332	0.320	0.326	0.328	0.320	0.319	0.332	0.325	0.005	0.013	1.556
Mode 4	0.228	0.228	0.223	0.228	0.227	0.223	0.227	0.227	0.224	0.223	0.228	0.226	0.002	0.005	0.905
Mode 5	0.107	0.106	0.108	0.108	0.108	0.109	0.108	0.109	0.109	0.106	0.109	0.108	0.001	0.003	0.944
Mode 6	0.102	0.100	0.102	0.102	0.103	0.103	0.102	0.103	0.103	0.100	0.103	0.102	0.001	0.003	0.932
Mode 7	0.087	0.087	0.087	0.088	0.088	0.088	0.088	0.088	0.088	0.087	0.088	0.088	0.000	0.001	0.372
-	0.080	0.080	0.080	0.080	0.080	0.080	0.080	0.080	0.080	-	-	-	-	-	-

Table 5.4: Extracted wavelength on displacements, velocities, and accelerations (1/wavenumber of tab.6.1).

From those values we see that mode 2 and 3 corresponds to about to 1/3 of mode 1 wavelength (1.5 periods on the axis), mode 4 about ¼ (2 periods), modes 5 and 6 about 1/10 (5 periods) and mode 7 about 1/12 (6 periods).

However, those numbers are not commensurable as there normally are in classical textbooks (for pure sine).
For a simple theoretical mechanical system with well-defined Dirichlet boundary conditions (at fixed position pinned axis ends with rotational freedom) those wavelengths can be easily interpreted as the distance between all zero-crossing locations. For Newmann boundary conditions this is not so obvious, as those boundaries imposes their own axis shape, and the distance between the zero-crossing are smaller and not uniform (but must be symmetric around the axis middle and is relevant for more than 2 zero-crossing). To underscore this, shapes of a spatially vibrating beam with both conditions are depicted in **Fig.5.1.** [13]. Moreover, a real mechanical system, even if simulated, has much more complex behaviour as we can observe on **Fig.3.2. and 3.4**, the wheel-rail contact point has some freedom to move and rotate, the wheels distort and have their own vibration modes etc. The right approach to study such a system is probably to consider the boundary as a mix between a pinned and clamped condition. A pinned wheel-rail with a spring and a clamped wheel-axis. A way to minimise those boundaries effects on extractions can be to avoid the data on the borders where the shape goes away from a sine (in our study we exclude the sensors S01 and S22). Based on all those considerations, we expect that the extracted wavelength may represent a situation in-between those extremes. Going deeper requires a more detailed analysis which is beyond the scoop of this paper.

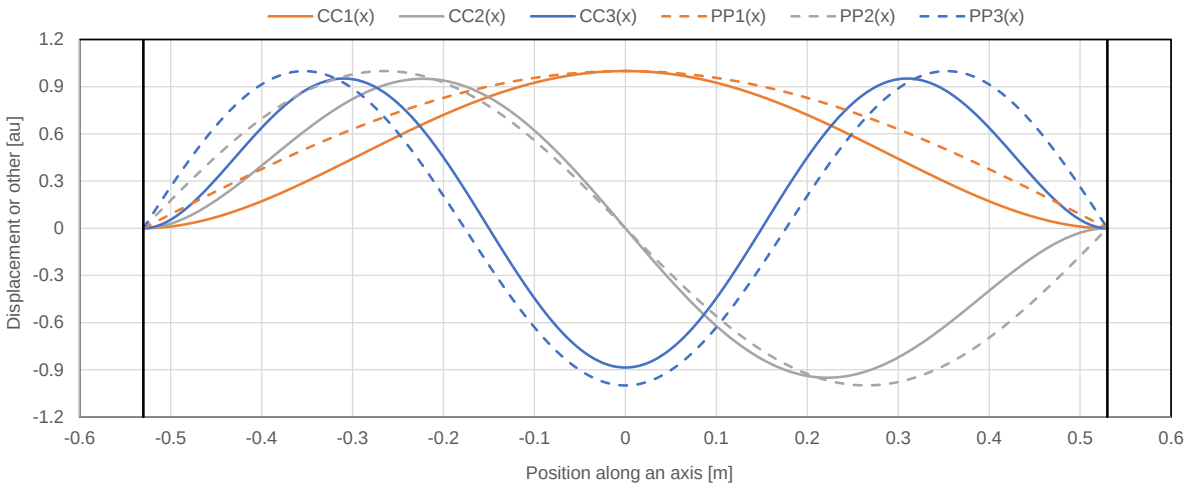

Figure 5.1. Shapes comparison of the first 3 vibrating beam modes with Dirichlet (PP = pinned-pinned, rotational free) and Newmann (CC = clamped-clamped, no possible rotation) boundary conditions [13].

5.2 Temporal results

Temporal modes are somehow more complicated and easier to analyse. The easiest part is that we consider only oscillations or perturbations without boundary conditions as for the space dimension (we start from an amplitude extremum which monotonically decrease). The complicate part concerns the temporal dimension, we have signals including tens to hundreds of modes (let us call it the temporal complexity, for this axis-wheels-railroad example we extracted 324 z acceleration modes, meaning a maximum 324/2=162 oscillators). The classification/analysis cannot be done manually anymore, and to perform it we introduced the kernel density spectrum (KDS) in [1].
We want to extract the density of all appearing modes for all 9 cases (displacements, velocities, and accelerations in all 3 spatial dimensions). We will use a simple gaussian kernel without any other coefficients except h which is the kernel smoothing parameter, also sometimes called bandwidth. F is an independent frequency parameter/range having a resolution of ΔF and F_k are the HODMD extracted mode frequencies:

$$KDS_G(F) = \frac{1}{n}\sum_{k=1}^{n} exp\left(\frac{-1}{2}\left(\frac{F - F_k}{h}\right)^2\right) \qquad (12)$$

By adequately choosing the bandwidth ($h < desired\ resolution$), the frequency resolution ($\Delta F < h$), and adequately norm the spectrum we can implement a multiscale resolution spectrum fitted to a specific problem. The KDS returns a smooth curve where the peaks representing a “center of gravity” of the nearby modes can easily be found and tracked. Adequate norming allows an estimation of the number of modes “attracted” by it through its amplitude.
The computational effort depends on the resolution and the frequency range we want to observe.

As example we use extracted modes from accelerations, velocities, and displacements in all 3 direction and plot the kernel density spectrums with different bandwidth parameters on **Figures.5.2. to 5.4.** We used the absolute values of all extracted frequencies as their appear in pears for oscillators, the norming is done simply by dividing the density by 18 (3 directions X 3 values X 2 signs). When a peak value is higher than 1, more than a single oscillator appears in this “gravitational field”, for peaks smaller than 1, not enough modes are present for a clean unique oscillator state. Increasing the bandwidth will enlarge the frequency “gravitational range”, smear the “spectrum”, and decrease the resolution. A correct understanding of the system and the required/targeted resolution remains therefore important.

Fig.5.2. shows on middle and bottom graphics that the lower frequencies (up to ≈ 4[kHz]) are more regular; at higher frequencies, the density spread is more important. On the top graphic the bandwidth is too large and the spectrum smears. A bandwidth in-between 0.5 and 1 [Hz] seems to be a good compromise in this case, but for real measurements it probably needs an adjustment.

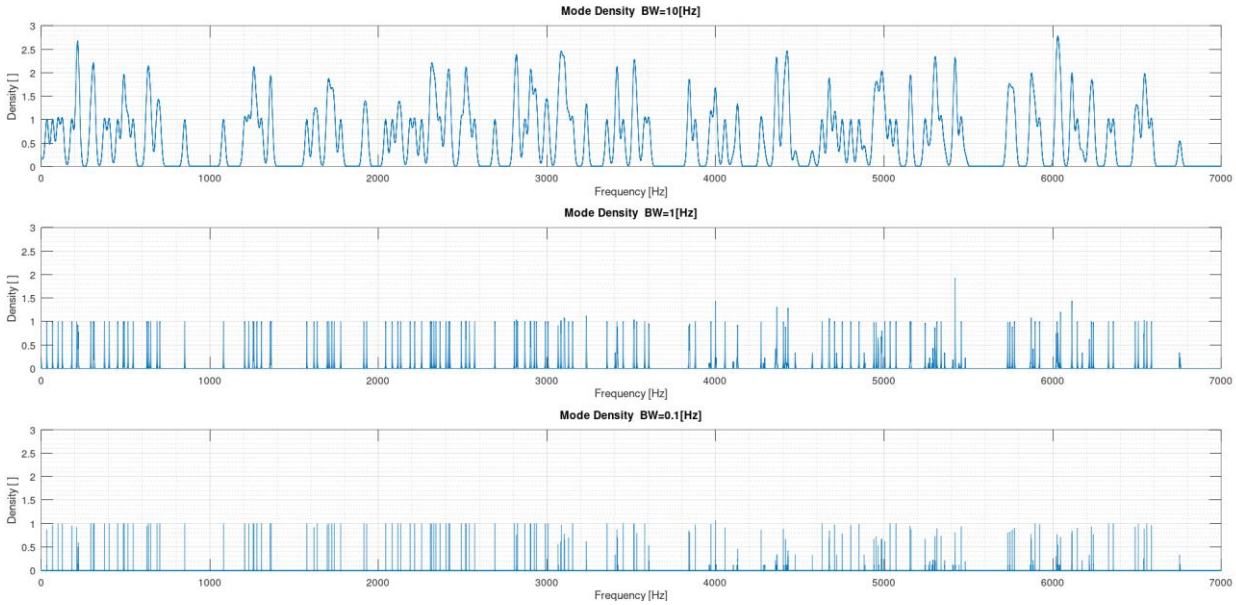

Figure 5.2. Mode densities for several kernel bandwidths (from top to bottom: 10[Hz], 1[Hz], 0.1[Hz])

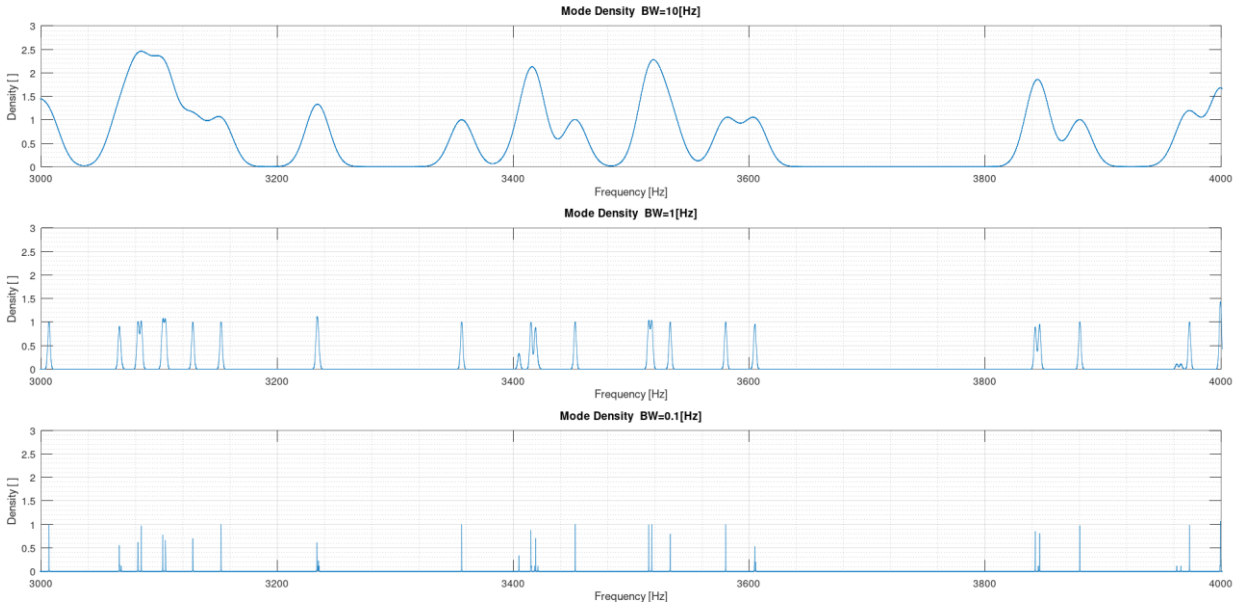

Figure 5.3. Frequency zooms of fig.6.3 (bandwidth from top to bottom: 10[Hz], 1[Hz], 0.1[Hz])

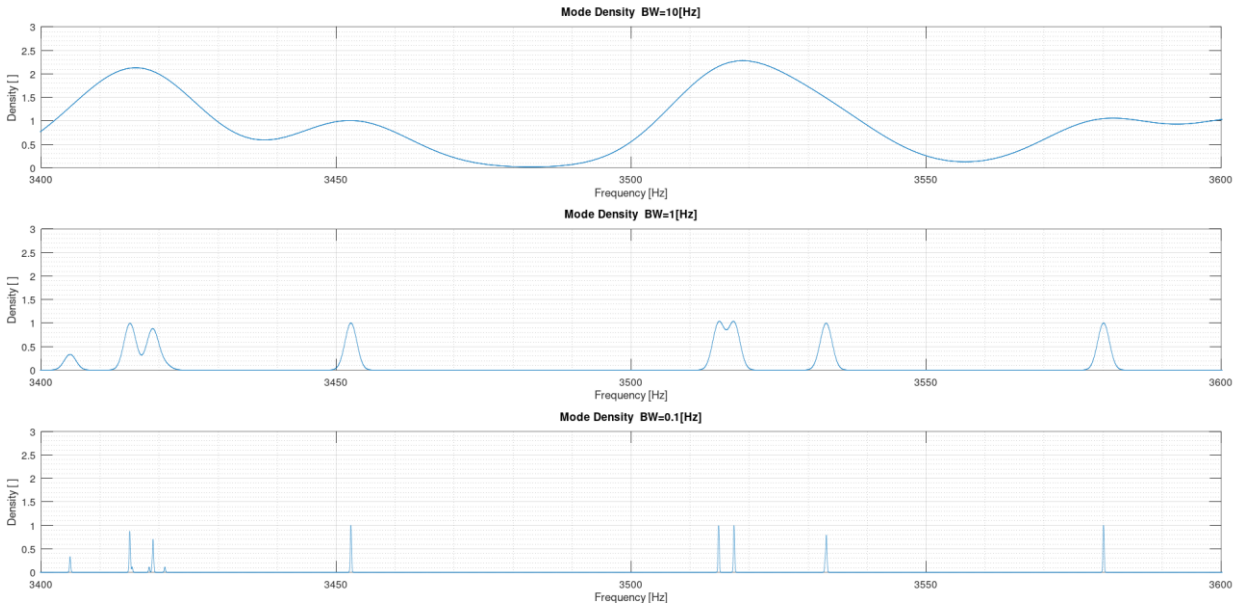

Figure 5.4. Frequency zooms of fig.6.4 (bandwidth from top to bottom: 10[Hz], 1[Hz], 0.1[Hz])

Merging the different modes, using a bandwidth (h) of 0.5 [Hz] for the kernel reduce the number of modes to 196 oscillators (eigenvector analysis performed directly on the mechanical system gave us 200 dominant modes). Filtering out those having an amplitude outside a 2% range around the normed amplitudes leads us to 108 oscillators (12% is required for +/- 1 mode).

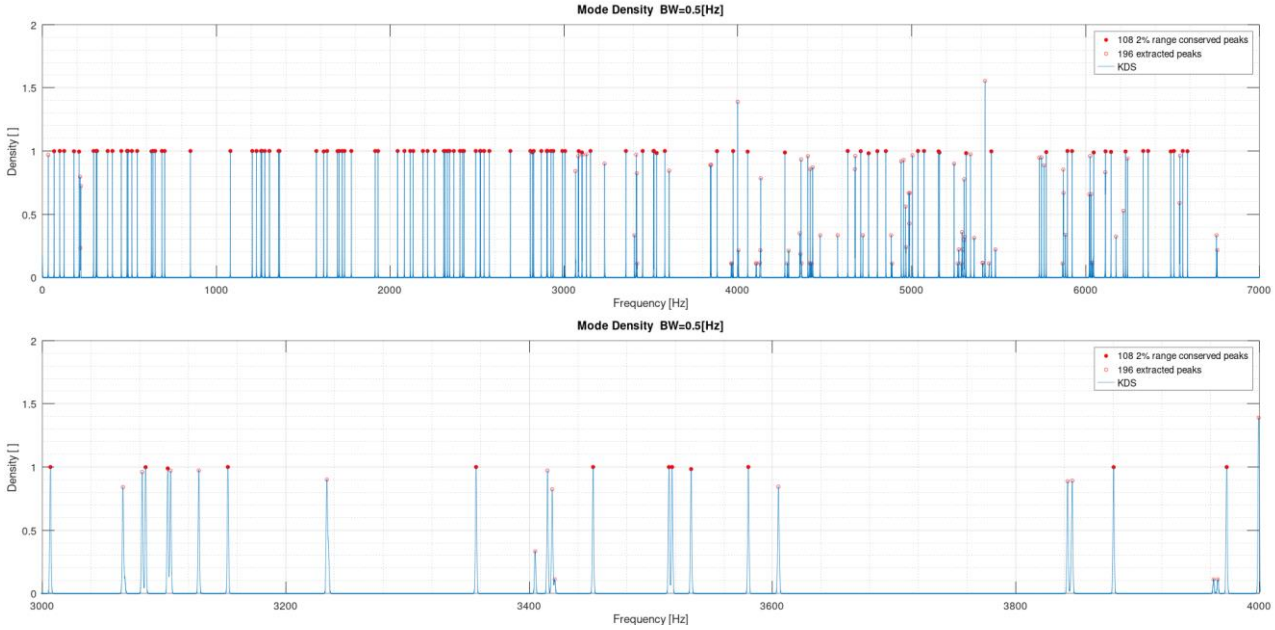

Figure 5.5. Merged and filtered modes (top: whole range, bottom: zoom)

The best strategy to follow is not clear yet. The main goal of this project is to verify if mechanical degradations (eg. cracks in the axis, bearing issues ect.) can be monitored by during operation by following the different measured modes. Based on the above extraction we may built a spectral base (of gaussians), one for each observed peak. Once this base has been built, we may have a first cornerstone.

Note 1: The above spectrum is built on a several of sensors along the axis. In a real situation, only a few sensors are placed on a sensor holder fixed at the axis end (not rotating and exited through a mechanical path including a cylinder gear, see **Fig.3.2.top**). For latest, a spectral base can be built on measurements performed over time.

Note 2: A clean spectral base should be a promising approach for a classification and identification of the different modes (remember HODMD delivers Dirac's which frequencies lives in $\mathbb{R}$). An identification of such pulses can be performed with a correlation to this base if latest does not change to abruptly.

Note 3: This base must be adapted over time to take into account the evolution of the mechanical system. The changes of the mechanical system may be analysed on the evolution of this base over time. An algorithm could be to correlate a new dataset to the existing base followed by an update of it.

Note 4: the major advantage over classical FFT or all transforms based on it, is that the spectrum is not smeared by the Lorenz kernel. The HODMD/KDS permits a multiscale resolution spectrum better adjustable to a specific problem.

6. Conclusions

This paper resume only a small part of a larger program consisting to evaluate data-driven signal processing methods for modal analysis of mechanical vibrations for preventive maintenance.

The main results we wanted to share at this point is that STKD seems a promising approach to process measurement performed on real mechanical systems and extract relevant and precise modal characteristics.

Next, we will try to analyse how-to best perform the HODMD-T-KDSB (higher order dynamic mode decomposition – truncation – kernel density spectrum base) on real measurements.

Glossary

ODE	Ordinary Differential Equation
PDE	Partially Differential Equations
FFT	Fast Fourier Transform
STFT	Short-Term Fourier Transform
PSD	Power Spectrum Density
DMD	Dynamic Mode Decomposition
HODMD	Higher Order Dynamic Mode Decomposition
STKD	Spatio-Temporal Koopman Decomposition
SVD	Singular Value Decomposition
KDE	Kernel Density Estimation
KDS	Kernel Density Spectrum

Fundings

This project was funded by Innosuisse project Nr. 37110.1 IP-ENG during my time at the FHNW-ISE.
The project is in closed status.

Since I left FHNW, I continue to work in the field of data-driven signal process for continuous education.
I use some of the data gathered during this project with the agreement of the previous project partners[2,3].
Since the end of the project this work is not funded and I spend private continuous education time on it.

Competing interests

The author declare he has no competing interests in this work.

Contributions

[1] Developed this procedure and compiled this manuscript.
[2,3] Contributed by delivering measurements, simulations, and remarks

[2] Fachhochschule Nordwestschweiz
Institut für Sensorik und Elektronik, (FHNW-ISE)
Institut für Produkt- und Produktionsengineering, (FHNW-IPP)
Klosterzelgstrasse 2, CH-5210 Windisch

[3] Vibro-Consult AG, Mess- und Schwingungstechnik
Stahlrain 6, CH-5200 Brugg

Acknowledgments

The author wishes to thank former colleagues for the possibility to work on this subject.

Availability of data and materials

The data is not available to the public due to confidentiality reasons.

Authors' remark

It may happen I uses some nice formulated sentences taken from the references. The subject is so broad and deep, and details may be very complex, that it will be impossible to cover it within a paper and remember exactly where all gathered information were obtained from. If I forgets citations or references, I ask for indulgence. Moreover, I avoided too complex mathematical formulations and try to give a more intuitive feeling of this method. If the reader wants to understand the deepness of the subject (which, honestly, I do not understand myself) there is no possible shortcuts to read and apply.
Unfortunately, since the project ended, I am limited to the dataset already available. Even for the simulations, I cannot generate new/complemental dataset because it was performed with a commercial software (ADINA 9.6.0) for which I have no licence neither the original simulation files (this task was perform by another group).
I envisage to build my one mechanical model using free open tools, but this will be verry time consuming until all is set up, so I decided to focus on existing dataset first and try to extract all what is possible from it. The good side is that, being unable to "rapidly try something else", it pushes me to stay creative to use what is available.

References

[1] Andreas Tuor & al
High Order Dynamic Mode Decomposition for Mechanical Vibrations and Modal Analysis
HAL Open Archive, https://hal.science/hal-04058070

[2] J.M. Vega and S. Le Clainche
Higher Order Dynamic Mode Decomposition and Its Applications
Elsevier Academic Press, ISBN: 978-0-12-819743-1, 2021

[3] S. Le Clainche & J. Vega
Higher Order Dynamic Mode Decomposition,
https://epubs.siam.org/doi/10.1137/15M1054924

[4] S. Le Clainche
DMD-based methods to identify flow patterns
AFMS Webinar 2020#16 video
https://www.dideo.tv/v/yt/DjTk73Q_Gsg/afms-webinar-2020-%2316-dr-soledad-le-clainche

[5] S.L. Brunton & J.N. Kutz
Data-Driven Science and Engineering, Machine Learning, Dynamical Systems, and Control
Cambridge University Press, DOI: 10.1017/9781108380690, 2019

[6] J.N. Kutz, S.L. Brunton, B.W. Brunton and J.L. Proctor
Dynamic Mode Decomposition, Data-Driven Modeling of Complex Systems
SIAM, Society for Industrial and Applied Mathematics, 2016

[7] S. Brunton, youtube video page (April 14, 2022)
https://www.youtube.com/c/Eigensteve/videos

[8] S.L. Brunton, B.W. Brunton, J.L. Proctor & J.N. Kutz
Koopman Invariant Subspaces and Finite Linear Representations of Nonlinear Dynamical Systems for Control
https://doi.org/10.1371/journal.pone.0150171

[9] H.Arbabi
Introduction to Koopman operator theory of dynamical systems
https://www.mit.edu/~arbabi/research/KoopmanIntro.pdf

[10] M.Gavish and D.L.Donoho
The Optimal Hard Threshold for Singular Values is 4/√3
IEEE Transaction on Information Theory, Vol. 60, No. 8, August 2014

[11] F.Ma, A.Imam & M.Morzfeld
The decoupling of damped linear systems in oscillatory free vibrations
Journal of Sound and Vibrations 324 (2009), pp.408-428

[12] Kathleen Champion, Peng Zheng, Aleksandr Aravkin, Steven L. Brunton & Nathan Kutz
A Unified Sparse Optimization Framework to Learn Parsimonious Physics-Informed Models From Data
https://www.researchgate.net/

[13] Robert D. Blevins
Formulas for natural frequency and mode shape.
Van Nostrand Reinhold Compagny, 1979

[14] Dynamic mode decomposition (April 14, 2022)
https://thereaderwiki.com/en/Dynamic_mode_decomposition